Bioorg. Med. Chem. 33 (2021) 116019

Contents lists available at ScienceDirect

Bioorganic & Medicinal Chemistry

journal homepage: www.elsevier.com/locate/bmc

Synthesis and structure-activity relationships of pyrimidine derivatives as potent and orally active FGFR3 inhibitors with both increased systemic exposure and enhanced *in vitro* potency

Ikumi Kuriwaki [a,*], Minoru Kameda [a], Kazuhiko Iikubo [a], Hiroyuki Hisamichi [a,1], Yuichiro Kawamoto [a,2], Shigetoshi Kikuchi [a,3], Hiroyuki Moritomo [a], Yutaka Kondoh [a,4], Tadashi Terasaka [a,5], Yasushi Amano [a], Yukihiro Tateishi [a], Yuka Echizen [a], Yoshinori Iwai [b], Atsushi Noda [b], Hiroshi Tomiyama [b], Taisuke Nakazawa [a], Masaaki Hirano [a]

[a] Drug Discovery Research, Astellas Pharma Inc., 21 Miyukigaoka, Tsukuba, Ibaraki 305-8585, Japan
[b] Research Laboratories, Kotobuki Pharmaceutical Co., Ltd., 198 Kamigomyou Sakaki-Machi, Hanishina-Gun, Nagano 389-0697, Japan

ARTICLE INFO

Keywords:
Fibroblast growth factor receptor 3
Bladder cancer
Antitumor effect
X-ray crystal structure
Molecular dynamics simulation
Structure–activity relationships

ABSTRACT

Fibroblast growth factor receptor 3 (FGFR3) is an attractive therapeutic target for the treatment of patients with bladder cancer harboring genetic alterations in FGFR3. We identified pyrimidine derivative **20b**, which induced tumor regression following oral administration to a bladder cancer xenograft mouse model. Compound **20b** was discovered by optimizing lead compound **1**, which we reported previously. Specifically, reducing the molecular size of the substituent at the 4-position and replacing the linker of the 5-position in the pyrimidine scaffold resulted in an increase in systemic exposure. Furthermore, introduction of two fluorine atoms into the 3,5-dimethoxyphenyl ring enhanced FGFR3 inhibitory activity. Molecular dynamics (MD) simulation of **20b** suggested that the fluorine atom interacts with the main chain NH moiety of Asp635 via a hydrogen bond.

1. Introduction

The recent development of molecular targeted therapeutics, which target specific cancer cell environment, has reduced the side effects of anticancer drugs and the burden on patients. For this reason, use of molecular targeted drugs has increased in clinical practice.[1] Tyrosine kinases are one of the main targets of these drugs, and many inhibitors have been discovered.[1] Representative molecular targeted drugs against tyrosine kinases include dacomitinib (EGFR/HER inhibitor), larotrectinib, entrectinib (NTRK1/2/3 inhibitor), lorlatinib (ALK inhibitor), pexidartinib (CSF1R inhibitor), and gilteritinib (FLT3 inhibitor), which have been approved since 2018.[1,2] However, while the efficacy of these agents is attractive for patients with a certain genetic background, they are not effective in all cancer patients. Therefore, there remain unmet medical needs in molecular targeted therapy.

Fibroblast growth factor receptor (FGFR) is a tyrosine kinase, and the fibroblast growth factor (FGF)/FGFR signaling pathway is known to play an important role in the development of various organs, in particular, in the process of cell proliferation and angiogenesis.[3] Abnormal activation of this pathway disrupts these processes in a subset of cancer patients. Genetic abnormalities, such as amplification, point mutations, translocation, and fusion genes of FGFRs, activate this pathway.[4–8] Such FGFR ablation is observed in lung cancer, breast cancer, multiple myeloma, uterine cancer, stomach cancer, brain tumor, bile duct cancer, and urothelial cancer.[9]

Drug discovery targeting FGFRs has been actively conducted in recent years, and a number of ongoing clinical trials are being conducted on drug candidates with selective FGFR inhibitory activity.[10,11] Some of

* Corresponding author.
E-mail address: ikumi.kuriwaki@astellas.com (I. Kuriwaki).
[1] Industrial Property Cooperation Center, Fukagawa Gatharia W3 Building, 1-2-15 Kiba, Koto-ku, Tokyo 135-0042, Japan.
[2] School of Life Sciences, Tokyo University of Pharmacy and Life Sciences, 1432-1 Horinouchi, Hachioji, Tokyo 192-0392, Japan.
[3] Tsukuba Research Laboratories, Tokuyama Corporation, 40 Wadai, Tsukuba, Ibaraki 300-4247, Japan.
[4] Kishida Chemical Co., Ltd., 13-2 Ooaza-hoshinosato, Ami-machi, Inashiki-gun, Ibaraki 300-0326, Japan.
[5] Japan Agency for Medical Research and Development, 1-5-5 Nihonbashi-muromachi, Chuo-ku, Tokyo 103-0022, Japan.

https://doi.org/10.1016/j.bmc.2021.116019
Received 27 November 2020; Received in revised form 8 January 2021; Accepted 11 January 2021
Available online 16 January 2021

these include AZD4547[12], infigratinib (NVP-BGJ398)[13], derazantinib (ARQ087)[14], pemigatinib (INCB054828)[15], E7090[16], and Debio1347 (CH5183284)[17], which target FGFR1, 2, and 3, and erdafitinib (JNJ-42756493)[18], rogaratinib (BAY1163877)[19], PRN1371[20], and futibatinib (TAS-120)[21], which are pan-FGFR inhibitors (Fig. 1). Among these drug candidates, erdafitinib has received approval from the U.S. Food and Drug Administration (FDA) for the treatment of adults with locally advanced or metastatic urothelial carcinoma harboring FGFR3 point mutations or fusion genes.[22,23] In addition, several compounds, such as infigratinib, derazantinib, pemigatinib, Debio1347, rogaratinib, and futibatinib have shown good results in clinical trials for intrahepatic cholangiocarcinoma (iCCA) patients with FGFR2 gene fusions.[24] Therefore, FGFRs are promising targets for treating patients with various types of cancer.

We previously reported that the lead compound **1**[25] (Fig. 2) had potent pan-FGFR inhibitory activity with excellent selectivity over VEGFR2 (Table 1). However, **1** showed low *in vitro* cell growth inhibitory activity against UM-UC-14 human bladder cancer cells endogenously expressing FGFR3 S249C (an activating gene point mutation) with an IC_{50} value of 84 nM[25] and NIH/3T3 cells exogenously overexpressing FGFR3 S249C with an IC_{50} value of 99 nM. In addition, plasma concentrations of **1** were low (98.2 nM) 6 h after oral administration of a 30 mg/kg dose to Institute of Cancer Research (ICR) mice. Given that the relationship between compound's plasma concentration and *in vitro* cellular activity, it would be necessary to improve both the *in vitro* cellular potency and systemic exposure to obtain a potent antitumor effect *in vivo* in a bladder cancer xenograft mouse model.[16,18] Therefore, we conducted a study to optimize pyrimidine derivatives to overcome these problems in **1**.

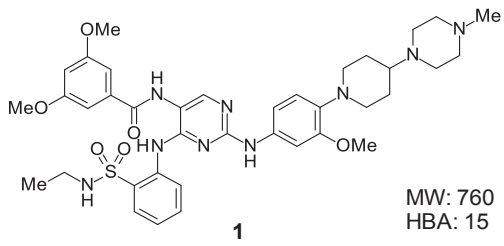

Fig. 2. Structure of compound **1**.[25]

Here, we describe the synthesis and biological evaluation of a novel series of pyrimidine derivatives and studies on their structure–activity relationships (SARs) using X-ray crystal structure to acquire potent and orally active pan-FGFR inhibitors with a different chemical structure from known FGFR inhibitors. Furthermore, we discuss their SARs based on molecular dynamics (MD) simulations.

2. Design and chemistry

2.1. Design

To begin compound design, we first confirmed the physical properties and metabolic stability of **1**. Compound **1** showed low permeability as indicated in the parallel artificial membrane permeability assay (PAMPA), poor aqueous solubility in the Japanese Pharmacopoeia 2nd fluid (JP2) test, and high *in vitro* intrinsic clearance in ICR mouse liver

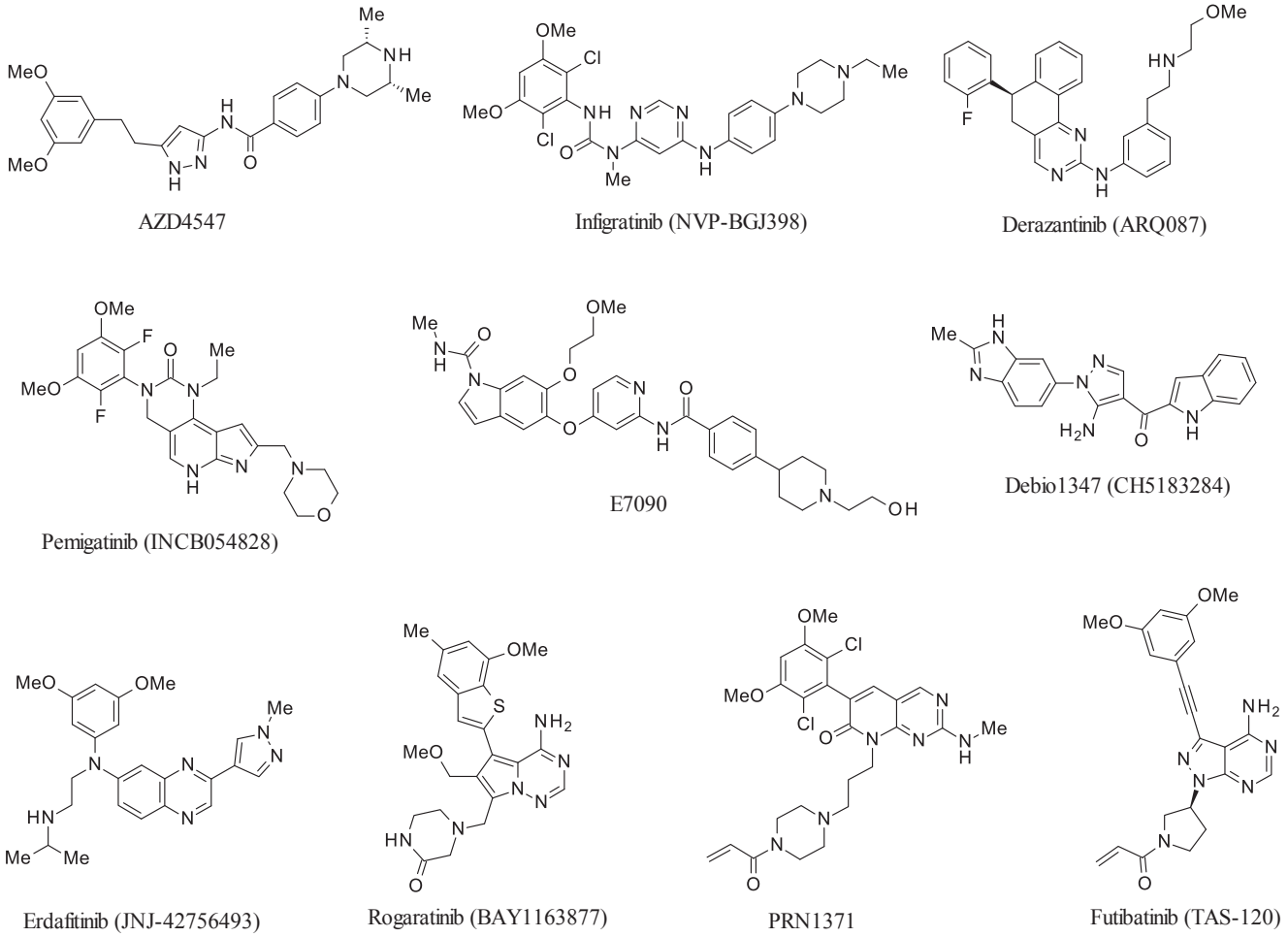

Fig. 1. Structure of known FGFR inhibitors examined in clinical studies.[10,11]

Table 1
In vitro potency and mouse plasma concentration of **1**.

Enzyme IC_{50} (nM)[a]					Cellular IC_{50} (nM)		Plasma Conc. (nM)[c]
FGFR1	FGFR2	FGFR3	FGFR4	VEGFR2	UM-UC-14[a]	NIH/3T3 (FGFR3 S249C)[b]	
2.1	3.1	4.3	74	>1000	84	99	98.2

[a] Data from reference 25.
[b] NIH/3T3 cells exogenously overexpressing FGFR3 S249C.
[c] Plasma concentration was measured using LC-MS/MS 6 h after single oral administration of **1** at 30 mg/kg to ICR mice (average of 3 mice).

microsomes (Tables 2 and 5). We judged that improving both permeability and aqueous solubility by adjusting lipophilicity would be difficult. Therefore, we optimized compounds with lower molecular weight (MW) and fewer hydrogen bond acceptors (HBAs) by applying the Lipinski's rule of five as a reference for drug-likeness.[26,27] An improvement in metabolic stability was also expected.

Our synthetic strategy was based on the X-ray complex crystal structure of FGFR3 with **2**[25], which is an analog of **1** (Fig. 3). The crystal structure indicated that three substructures were maintained: (1) the 2-aminopyrimidine group (two hydrogen bond interactions with Ala558, located in the hinge region of the ATP binding site); (2) the dimethoxyphenyl group (van der Waals (vdW) interaction with Met529 in the back pocket, which contributes to FGFR selectivity over VEGFR2[25]); (3) the 4-(4-methylpiperazin-1-yl)piperidin-1-yl-benzene group (available substructure in the solvent region of some kinase inhibitors such as gilteritinib[28] (FLT3/AXL inhibitor), ASP3026[29] (EML4-ALK inhibitor), and naquotinib[30] (EGFR T790M inhibitor)). In contrast, the *N*-ethyl-2-sulfamoyl-anilino group, which fills the sugar pocket and interacts with Lys508 via a hydrogen bond, had not been optimized. Therefore, we planned to replace this unit with smaller substituents to decrease MW and HBA values (Fig. 3).

The detailed strategy is shown in Fig. 4. First, compounds were designed to partially or completely reduce the size of the *N*-ethyl-2-sulfamoyl-anilino unit (shown in red) of **1**. Next, we considered optimizing the linker between the 3,5-dimethoxybenzene and pyrimidine (shown in blue) because the sulfamoyl group was located close to the linker, and conversion of the sulfamoyl group would affect the position of the 3,5-dimethoxybenzene. Because **2**[25] had an ethylene linker and

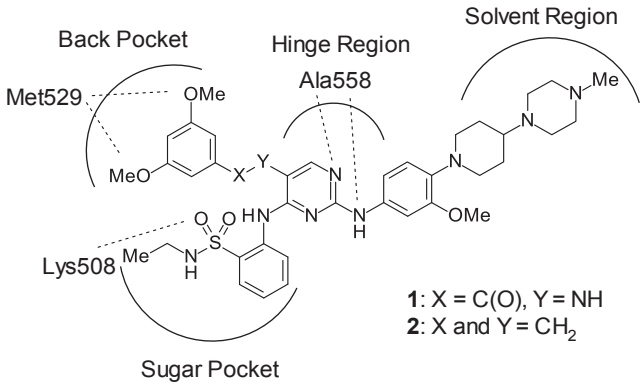

Fig. 3. Illustration of representative kinase pockets and amino acid residues with **1** and **2**.

Table 2
Results of optimizing a smaller structure for substituent R^3.

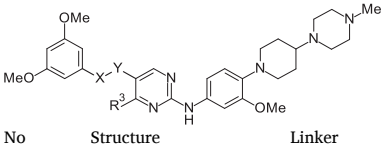

No	Structure R^3	Linker X	Linker Y	Enzyme FGFR3 IC_{50} (nM)	Cellular FGFR3 IC_{50} (nM)[a]	PAMPA (10^{-6} cm/sec)[b]	Solubility (μM)[c]	Log $D_{7.4}$	MW[d]	HBA[d]
1	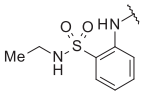	C(O)	NH	4.3[e]	99	1.4	<1	>3.9	760	15
7a		C(O)	NH	467	NT	0.4	36	3.7	653	12
7b	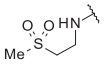	C(O)	NH	>1000	NT	<0.2	≥100	1.8	683	14
7c	H	C(O)	NH	>1000	NT	<2.9	≥100	2.8	562	11
2	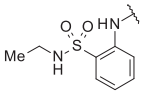	CH_2	CH_2	2.8[e]	34	1.8	<1	>4.8	745	13
11	H	CH_2	CH_2	24	324	15.1	≥100	3.5	547	9

[a] NIH/3T3 cells exogenously overexpressing FGFR3 S249C.
[b] Parallel artificial membrane permeability assay (PAMPA) at pH = 6.5.
[c] Aqueous solubility in the Japanese Pharmacopoeia 2nd fluid (JP2) for disintegration test (pH = 6.8 buffer).
[d] MW and HBA values were calculated using ACD/Percepta (ver. 2018.2.5) software.
[e] Data from reference 25.

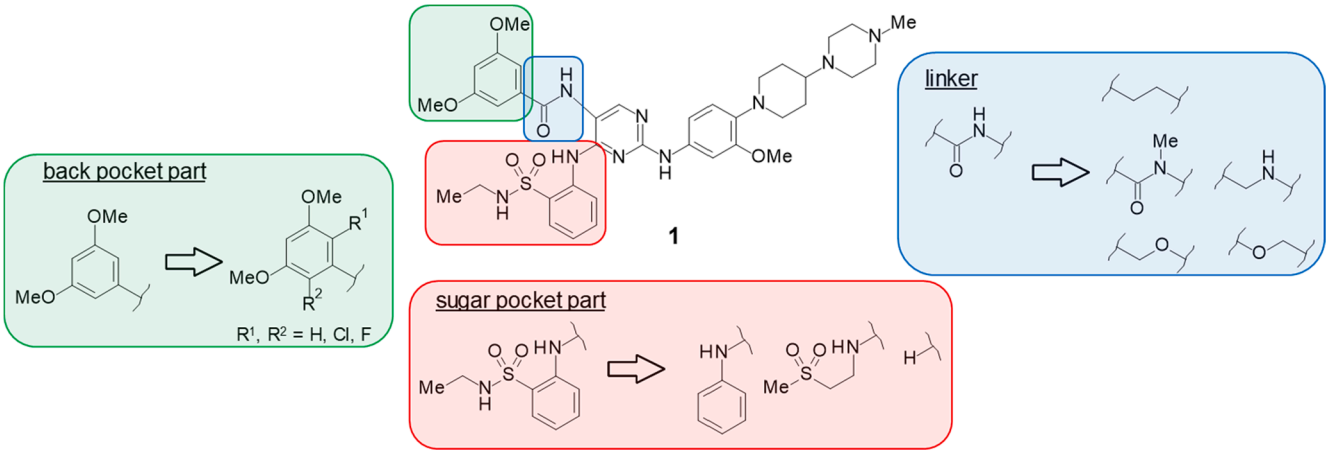

Fig. 4. Synthetic plan.

exhibited similar potency to **1** against FGFR3, we introduced linkers consisting of various combinations of pairs of atoms including an ethylene unit. Finally, according to a reported strategy for enhancing FGFR inhibitory activity[13], we introduced various halogen atoms into 3,5-dimethoxybenzene (shown in green).

2.2. Chemistry

Synthesis of the target compounds is outlined in Schemes 1–4. Synthesis of compounds **7a–d** is shown in Scheme 1. Compounds **3a–c** were introduced to commercially available **4** via a nucleophilic aromatic substitution (S_NAr) reaction under acidic conditions to give **5a–c**. Reduction of the nitro groups of **5a–c** gave **6a–c**, which were treated with 3,5-dimethoxybenzoyl chloride or condensed with 3,5-dimethoxybenzoic acid to give **7a–c**. Compound **7d** was synthesized from **6c** via reductive amination reaction with 3,5-dimethoxybenzaldehyde.

Scheme 2 shows the synthesis of compound **11**. Commercially available **8** was reacted with **4** via an S_NAr reaction to give **9**, which was subsequently coupled with 1-ethynyl-3,5-dimethoxybenzene via Sonogashira reaction[31] to yield **10**. The alkyne linkage of **10** was reduced by adding hydrogen to give **11**.

Compounds **14a–c** were synthesized according to Scheme 3. Compound **12a** was reacted with 3,5-dimethoxybenzoyl chloride to give **13a**, whose amide moiety was methylated using iodomethane to give **13b**. Compound **13c** was synthesized by introducing 3,5-dimethoxyphenol to **12b** via Mitsunobu reaction[32,33] to yield **13c**. Alkylation of the phenolic hydroxyl group in **12c** using 3,5-dimethoxybenzyl bromide gave **13d**. Compounds **13b–d** were converted to **14a–c** using Buchwald reaction condition[34].

Synthesis of compounds **20a–d** is shown in Scheme 4. Chlorination of **15** using SO_2Cl_2 gave **16a**. Fluorination of **15** using Selectfluor™ gave **16b** and **16c**. Compound **16c** was chlorinated to yield **16d**. Compound **17** was reacted with **4** under microwave (μW) irradiation via an S_NAr reaction to give **18**, which was alkynylated with **16a–d** via Sonogashira reaction[31] to give **19a–d**. The alkyne moiety of **19a–d** was hydrogenated by *in-situ* generation of a diimide[35] to yield **20a–d**.

3. Results and discussion

Synthesized compounds were evaluated using an ADP-Glo luminescent kinase assay with human recombinant FGFR3 enzyme. Some compounds were assessed using a cell growth assay in NIH/3T3 cells exogenously overexpressing FGFR3 S249C. In addition, selected compounds were assessed by examining permeability, aqueous solubility, metabolic stability, plasma concentration, and/or *in vivo* inhibitory activity against phosphorylation of FGFR3.

Table 2 shows the SAR of the substituent R^3 of **1** and **2**. Compared to **1**, **7a–c** had over 100-fold lower FGFR3 enzyme inhibitory activity,

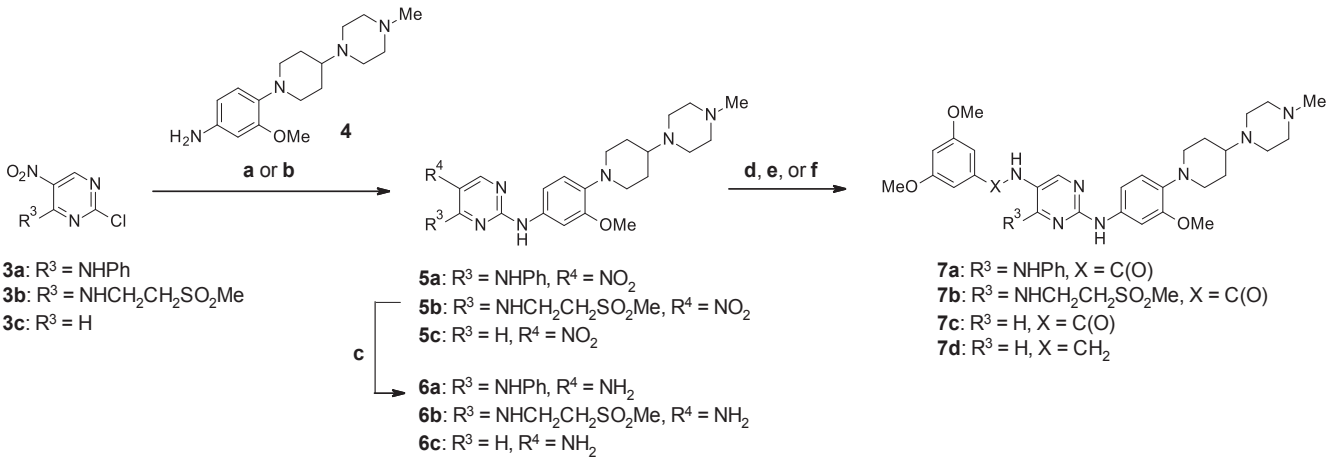

Scheme 1. Reagents and conditions: (a) **4**, AcOH, room temperature, 62–84% for **5a** and **5b**; (b) **4**, MsOH, EtOH, 100 °C, 63% for **5c**; (c) H_2, Pd/C, EtOH/THF or EtOH, room temperature, 71–100%; (d) 3,5-dimethoxybenzoyl chloride, DIPEA, THF, room temperature, 30% for **7a**; (e) 3,5-dimethoxybenzoic acid, HATU, DIPEA, DMF, room temperature, 33–51% for **7b** and **7c**; (f) (i) 3,5-dimethoxybenzaldehyde, $NaBH(OAc)_3$, CH_2Cl_2, room temperature, (ii) $NaBH_4$, MeOH, room temperature, 16% (2 steps) for **7d**.

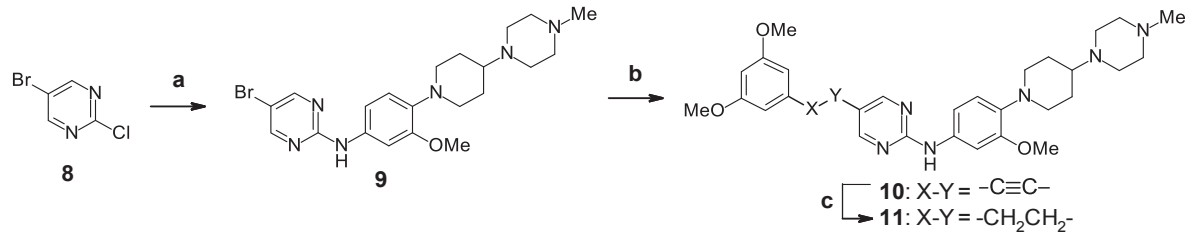

Scheme 2. Reagents and conditions: (a) **4**, MsOH, IPA, 90 °C to 110 °C, 79%; (b) 1-ethynyl-3,5-dimethoxybenzene, $Pd(PPh_3)_4$, CuI, Et_3N, DMF, 110 °C, 93%; (c) H_2 (3 atm), Pd/C, MeOH/THF, room temperature, 54%.

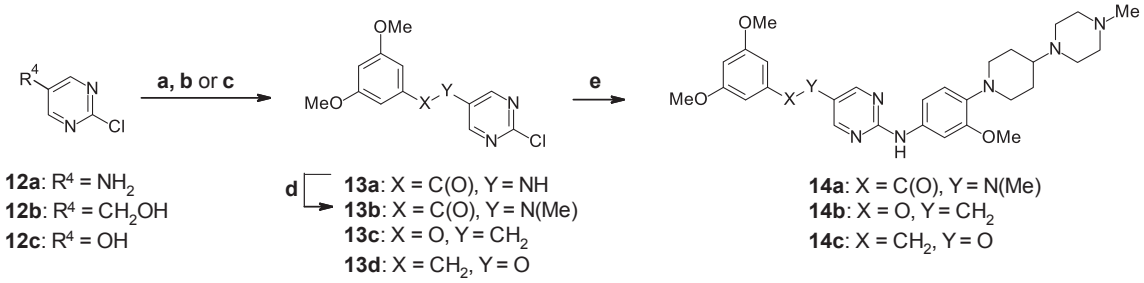

Scheme 3. Reagents and conditions: (a) 3,5-dimethoxybenzoyl chloride, DIPEA, THF, room temperature, 77% for **13a**; (b) 3,5-dimethoxyphenol, ADDP, *n*-Bu_3P, THF, room temperature, 53% for **13c**; (c) 3,5-dimethoxybenzyl bromide, K_2CO_3, DMF, room temperature, 60% for **13d**; (d) iodomethane, NaH, DMF, room temperature, 73%; (e) **4**, $Pd(OAc)_2$, *rac*-BINAP, Cs_2CO_3, 1,4-dioxane, 100 °C, 33–82%.

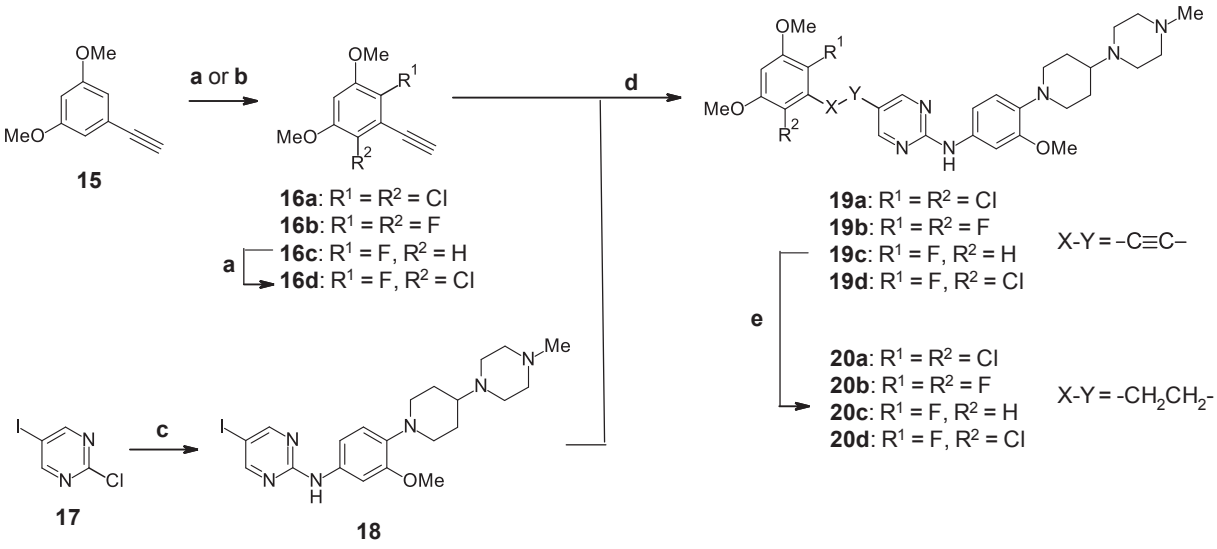

Scheme 4. Reagents and conditions: (a) SO_2Cl_2, MeCN, room temperature, 47–83% for **16a** and **16d**; (b) Selectfluor™, MeCN, room temperature, 20–31% for **16b** and **16c**; (c) **4**, MsOH, IPA, microwave (μW), 130 °C, 83%; (d) $Pd(PPh_3)_4$, CuI, DIPEA or Et_3N, DMF, 80 °C or 100 °C, 52–66%; (e) *p*-toluenesulfonyl hydrazide, NaOAc, DME/water, 110 °C, 24–69%.

whereas **11** showed 9-fold lower FGFR3 enzyme inhibitory activity than that of **2** (IC_{50} values were 24 nM and 2.8 nM, respectively). Moreover, the inhibitory activity of **11** against the proliferation of NIH/3T3 cells exogenously overexpressing FGFR3 S249C was 10-fold lower than that of **2** (IC_{50} values were 324 nM and 34 nM, respectively). With regard to physical properties, although the aqueous JP2 solubility of **7a–c** improved according to Log $D_{7.4}$ values, these compounds had poor permeability. In contrast, compared to the poor physical properties of **2**, **11** showed improved permeability and JP2 solubility. Considering that permeability is generally correlated with the lipophilicity, the improved permeability of **11** in contrast to **2** was possibly due to its lower MW (547) and HBA (9) among the two compounds.

Table 3 shows the SAR of the linker X and Y between the 3,5-dimethoxybenzene and pyrimidine of **11**. Compared to **11**, compounds **14a**, **14b**, and **7d** showed reduced FGFR3 enzyme inhibitory activity, whereas **14c** exhibited comparable activity. As for the physical properties, all compounds showed favorable JP2 solubility. The permeability of **7d** and **14c** was similar to that of **11**, whereas that for **14b** improved to over 30×10^{-6}cm/sec, possibly because of its smaller surface area.

Fig. 5 shows the X-ray crystal structure of **11** in complex with FGFR3. Similar to the interaction of **2** with FGFR3[25], the 2-aminopyrimidine unit of **11** formed hydrogen bonds with the main chain atoms of Ala558 in the hinge region. In addition, the 3,5-dimethoxyphenyl group formed hydrophobic and vdW interactions with the amino acid residues (Met529, Val555 and Ala634) in the back pocket. In addition, the ethylene linker was located in the hydrophobic region surrounded by the

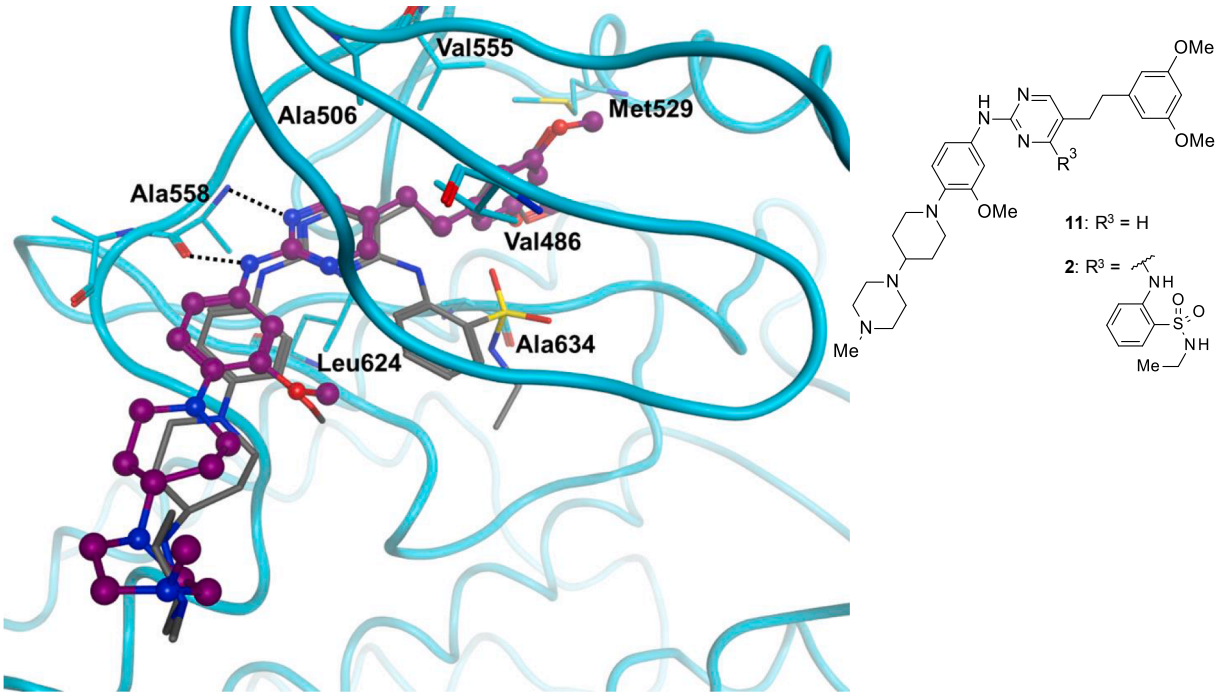

Fig. 5. X-ray crystal structure of **11** in complex with FGFR3 (PDB code: 7DHL). **2** is superimposed and shown as a stick model in grey.[25]

side chains of Val486, Ala506, Val555, Leu624, and Ala634. Our findings suggested that the interaction between **11** and these hydrophobic amino acids would cause **11** to exhibit potent kinase inhibitory activity. Meanwhile, other compounds (**7c**, **7d**, and **14a–c**) that contained some hetero atoms in the linker unit would not show such optimal hydrophobic interactions, indicated that they would exhibit lower potency than **11**. Based on both the potency and physical properties, ethylene was selected as the best linker for further optimization.

Table 4 shows the SAR of the 3,5-dimethoxyphenyl group of **11**. Although compound **20a**, which contained dichloro groups, showed 6-fold greater enzyme inhibitory activity than **11**, the increased lipophilicity significantly reduced the JP2 solubility. In contrast, compound **20b**, a difluoro derivative, showed very potent enzyme inhibitory activity with an IC_{50} value of 1.2 nM and cellular activity with an IC_{50} value of 13 nM (20 times and 25 times more potent than **11**, respectively). The JP2 solubility of **20b** was 79 μM and is expected to improve systemic exposure following oral dosing. Compound **20d**, which contained both fluorine and chlorine atoms, showed similar enzyme inhibitory activity to **20b**, but poor solubility comparable to **20a**. Furthermore, compound **20c**, a monofluoro derivative, showed lower enzyme inhibitory activity than that of **20b**, indicating that both fluoro groups of **20b** were important for potent kinase inhibitory activity. In addition, all compounds in this table showed good permeability similar to **11** due to their suitable Log $D_{7.4}$ values; therefore, cellular activity was mostly correlated with enzyme inhibitory activity among the compounds in Table 4.

With the aim of clarifying the effect of the fluoro atoms in **20b**, molecular dynamics (MD) simulation by GROMACS[37] was performed using the X-ray crystal structure of **11** in complex with FGFR3 as a template. Energy-minimized structures of **11**, **20a** and **20b** bound to FGFR3 were generated and used as a starting model. We focused on Cβ of Lys508, Cγ of Val555, Cβ of Ala634, and the main chain NH moiety of

Table 3
Results of changing the linker X and Y between the 3,5-dimethoxybenzene and pyrimidine.

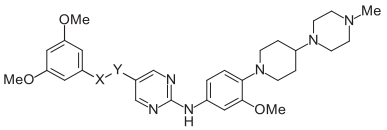

No	Linker		Enzyme FGFR3 IC_{50} (nM)	PAMPA (10^{-6} cm/sec)[a]	Solubility (μM)[b]	Log $D_{7.4}$	Surface area[c]
	X	Y					
11	CH_2	CH_2	24	15.1	≥100	3.5	610.2
14a	C (O)	N (Me)	>1000	3.7	≥100	1.8	624.7
14b	O	CH_2	380	>30.0	≥100	3.4	599.6
7d	CH_2	NH	78	18.1	≥100	2.9	603.3
14c	CH_2	O	45	18.5	≥100	3.2	602.0

[a] Parallel artificial membrane permeability assay (PAMPA) at pH = 6.5.
[b] Aqueous solubility in the Japanese Pharmacopoeia 2nd fluid (JP2) for disintegration test (pH = 6.8 buffer).
[c] Surface area values were calculated using Molecular Operating Environment (MOE)[36] software (average of 3 times).

Table 4
Results of optimizing substituents R^1 and R^2 in the 3,5-dimethoxyphenyl unit.

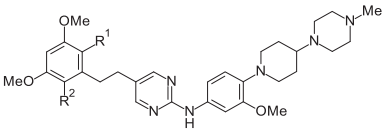

No	Structure		Enzyme FGFR3 IC_{50} (nM)	Cellular FGFR3 IC_{50} (nM)[a]	PAMPA (10^{-6} cm/sec)[b]	Solubility (μM)[c]	Log $D_{7.4}$
	R^1	R^2					
11	H	H	24	324	15.1	≥100	3.5
20a	Cl	Cl	4.3	113	18.7	5	4.4
20b	F	F	1.2	13	18.4	79	3.0
20c	F	H	5.2	95	24.4	≥100	3.2
20d	F	Cl	1.6	31	19.4	12	3.5

[a] NIH/3T3 cells exogenously overexpressing FGFR3 S249C.
[b] Parallel artificial membrane permeability assay (PAMPA) at pH = 6.5.
[c] Aqueous solubility in the Japanese Pharmacopoeia 2nd fluid (JP2) for disintegration test (pH = 6.8 buffer).

Asp635, which were located within 4.5 Å of the fluorine atoms substituted in the 3,5-dimethoxybenzene of **20b** in the model structure (Fig. 6**a**).

The frequency distribution of distances between each amino acid residue and the R^1/R^2 substitutions (hydro/chloro/fluoro) in the MD simulation are displayed in histograms in Fig. 6**b**. The histograms show that the distribution of distances interacting with Lys508 or Val555 was similar among the three compounds. These findings suggested that a more hydrophobic substituent was favorable for interacting with Lys508/Val555, explaining why **20a** and **20b** were more potent than **11**. In contrast, the distribution of distances interacting with Ala634 or Asp635 were different among compounds. A smaller R^1/R^2 substituent resulted in a shorter distance with Ala634, suggesting that Ala634 could avoid steric repulsion with the R^1/R^2 substituent. The fluorine substituent formed a shorter distance with Asp635 than hydrogen or chlorine substituents. These results suggested that the main chain NH moiety of Asp635 would interact with the fluorine atom via a hydrogen bond[38] because a fluorine atom has greater electronegativity than hydrogen or chlorine atoms[39]. This may also explain why **20b** showed improved FGFR3 inhibitory activity compared to **11** and **20a**. While **20d** exhibited similar potency to **20b**, the FGFR3 inhibitory activity of **20c** was lower than that of **20b**. These results suggested that the fluoro atom of **20d** would interact with Asp635 in same manner as that of **20b**, while a chloro substituent would additionally interact with Lys508/Val555. Moreover, it was speculated that the fluoro substituent of **20c** would interact with either Ala634/Asp635 or Lys508/Val555.

Table 5 shows the plasma concentration and *in vivo* inhibitory activity against FGFR3 phosphorylation of orally administered test compounds at 30 mg/kg, and *in vitro* intrinsic clearance in ICR mouse liver microsomes. Plasma concentrations were measured using LC-MS/MS 6 h after administration to ICR mice, and *in vivo* FGFR3 phosphorylation in tumors was measured using sandwich ELISA 6 h after administration to nude mice xenografted with NIH/3T3 cells exogenously overexpressing FGFR3 S249C. Both **11** and **20b** exhibited improved systemic exposure and lower values of *in vitro* metabolic stability than **1**. Moreover, **11** and **20b** showed 21% and 85% *in vivo* inhibitory activity against FGFR3 phosphorylation, respectively.

The higher plasma concentrations of **11** and **20b** were attributed to not only improved physical properties (PAMPA and JP2 solubility) but also improved *in vitro* metabolic stability. Moreover, **20b** exhibited more potent *in vivo* inhibitory activity against FGFR3 phosphorylation than **11**, suggesting that potent cellular activity of **20b** was necessary for potent *in vivo* activity.

Given the promising features of **20b**, including its high plasma concentration and potent *in vivo* FGFR3 inhibitory activity, further pharmacological evaluations were conducted (Table 6). Compound **20b** exhibited potent enzyme inhibitory activity against other FGFR subtypes with similar IC_{50} values to that for FGFR3. As for the kinase selectivity of **20b**, the enzyme inhibitory activity for FGFR3 was 28-fold more potent than that for VEGFR2 (IC_{50} value was 34 nM). Moreover, **20b** had potent cell growth inhibitory activity against the UM-UC-14 human bladder cancer cell line, with an IC_{50} value of 21 nM.

Finally, we evaluated an *in vivo* antitumor assay using a nude mouse model xenografted with UM-UC-14 bladder cancer cells (Table 7). Compound **20b** (0.1, 0.3, 1, 3, and 10 mg/kg) was suspended in vehicle (0.5% methylcellulose solution) and orally administered to mice once daily for 11 days. Tumor growth inhibition at doses of 0.3 mg/kg (48% inhibition) and 1 mg/kg (62% inhibition), and tumor regression at doses of 3 mg/kg (42% regression) and 10 mg/kg (75% regression) were observed in a dose-dependent manner. These pharmacological results suggest that **20b** is an orally active lead compound for the treatment of bladder cancer patients.

4. Conclusion

We conducted structural optimization of the lead compound **1** to explore potent and orally active FGFR3 inhibitors with increased systemic exposure and enhanced *in vitro* potency against FGFR3. Reducing the molecular size of the substituent at the 4-position and replacing the linker of the 5-position in the pyrimidine scaffold improved permeability, aqueous solubility and *in vitro* metabolic stability, and increased systemic exposure. Furthermore, introducing two fluorine atoms into the 3,5-dimethoxyphenyl ring enhanced FGFR3 inhibitory activity. MD simulation of **20b** indicated that the fluorine atoms would interact with Lys508, Val555, Ala634, and Asp635, and that particularly the main chain NH moiety of Asp635 would interact with the fluorine atom via a hydrogen bond. The resulting pyrimidine derivative **20b** induced tumor regression following oral administration to a bladder cancer xenograft nude mouse model. Further optimization studies on novel FGFR3 inhibitors derived from **20b**, as an orally active lead compound, will be reported in the future.

5. Experimental

5.1. Chemistry

^{1}H-NMR spectra were recorded on Varian 400, Varian VNS-400, or Varian 400-MR and chemical shifts are expressed in δ (ppm) values with tetramethylsilane as an internal reference (s = singlet, d = doublet, t = triplet, m = multiplet, dd = doublet of doublets, and br = broad peak). Mass spectra (MS) were recorded on Thermo Electron LCQ Advantage, Thermo Trace DSQ, Waters SQD, or Agilent Quadrupole. Electrospray ionization (ESI) positive high resolution mass spectra (HRMS) were obtained using Thermo Fisher EXACTIVE-Plus. Elemental analyses were performed with Yanaco MT-6 (C, H, N), Elementar Vario MICRO cube (C, H, N), Elementar Vario EL III (C, H, N), DIONEX DX-500 (S, halogen), DIONEX ICS-3000 (S, halogen), or DIONEX ICS-5000 (S, halogen) instruments, and the results were within ±0.4% of theoretical values. The following abbreviations are used: AcOH, acetic acid; MeCN, acetonitrile; HATU, O-(7-aza-1*H*-benzotriazol-1-yl)-*N,N,N′,N′*-tetramethyluronium hexafluorophosphate; ADDP, 1,1′-(azodicarbonyl)dipiperidine; BINAP, 2,2′-bis(diphenylphosphino)-1,1′-binaphthyl; IPE, diisopropyl ether; DIPEA, *N,N*-diisopropylethylamine; DME, 1,2-dimethoxyethane; DMSO, dimethyl sulfoxide; DMF, *N,N*-dimethylformamide; EtOH, ethanol; EtOAc, ethyl acetate; IPA, isopropyl alcohol; MsOH, methanesulfonic acid; MeOH, methanol; $Pd(OAc)_2$, palladium(II) acetate; NaOAc, sodium acetate; $NaBH(OAc)_3$, sodium triacetoxyborohydride; THF, tetrahydrofuran; *n*-Bu_3P, tri-*n*-butylphosphine; Et_3N, triethylamine; PPh_3, triphenylphosphine.

5.1.1. N^2-{3-Methoxy-4-[4-(4-methylpiperazin-1-yl)piperidin-1-yl]phenyl}-5-nitro-N^4-phenylpyrimidine-2,4-diamine (**5a**)

A mixture of 2-chloro-5-nitro-*N*-phenylpyrimidin-4-amine (**3a**, 260 mg, 1.04 mmol), 3-methoxy-4-[4-(4-methylpiperazin-1-yl)piperidin-1-yl]aniline (**4**, 316 mg, 1.04 mmol), and AcOH (4.00 mL) was stirred at room temperature overnight. The mixture was quenched with water, NaOH (1.0 M aqueous solution), and sat. $NaHCO_3$ *aq.* in an ice-water bath and extracted with $CHCl_3$. The organic layer was washed with brine, dried over $MgSO_4$ and concentrated *in vacuo*. The residue was purified by column chromatography on silica gel ($CHCl_3$/MeOH/28% NH_3 *aq.* = 100:0:0 to 90:9:1) to give the product (450 mg, 84%) as a red solid. ^{1}H NMR (400 MHz, DMSO-d_6) δ ppm 1.46–1.60 (2H, m), 1.72–1.88 (2H, m), 2.16 (3H, s), 2.20–2.58 (11H, m), 3.24–3.40 (2H, m), 3.42–3.56 (3H, m), 6.63–6.73 (1H, m), 7.03–7.17 (2H, m), 7.17–7.29 (1H, m), 7.30–7.44 (2H, m), 7.52–7.66 (2H, m), 9.08 (1H, s), 10.19–10.41 (2H, m); MS (ESI) *m/z* $[M + H]^+$ 519.

5.1.2. N^4-[2-(Methanesulfonyl)ethyl]-N^2-{3-methoxy-4-[4-(4-methylpiperazin-1-yl)piperidin-1-yl]phenyl}-5-nitropyrimidine-2,4-diamine (**5b**)

Compound **5b** was prepared from 2-chloro-*N*-[2-(methanesulfonyl)ethyl]-5-nitropyrimidin-4-amine (**3b**) and **4** in 62% yield using a similar

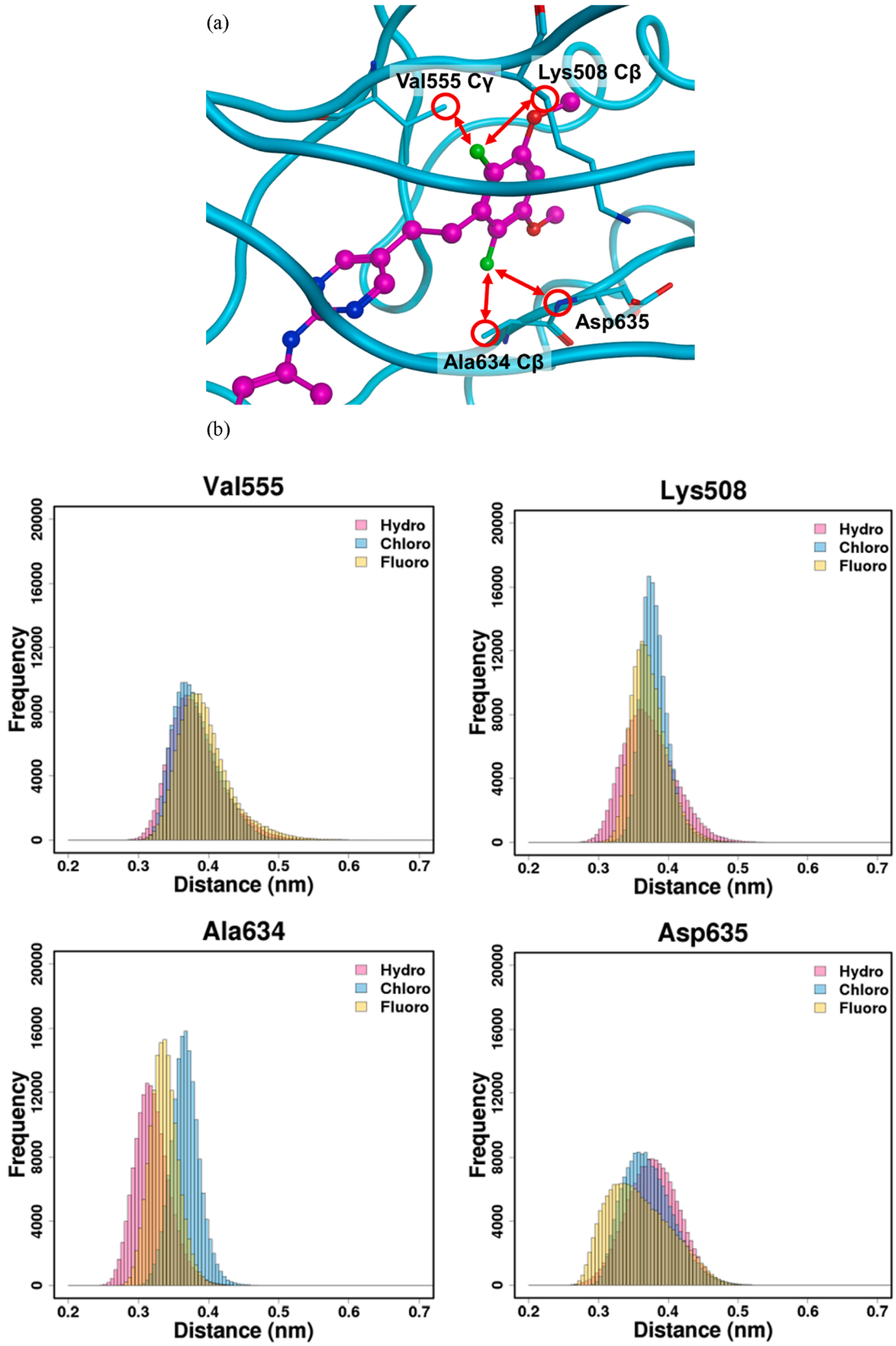

Fig. 6. Molecular simulations of **11**, **20a**, and **20b**. (a) The complex structure of **20b** docked with FGFR3 around the back pocket, and amino acid residues located within 4.5 Å of the fluorine atoms. (b) Frequency distribution of distances between the amino acid residues and R^1/R^2 substituents in an MD simulation.

Table 5
Plasma concentration, *in vivo* inhibitory activity against FGFR3 phosphorylation, and *in vitro* metabolic stability.

No	Structure	Plasma conc. (nM)[a]	*p*-FGFR3 (% inh.)[b]	CL_{int} (mL/min/kg)[c]	Cellular FGFR3 IC_{50} (nM)[d]	PAMPA (10^{-6} cm/sec)[e]	Solubility (μM)[f]
1	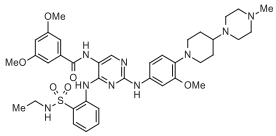	**98.2**	**NT**[g]	**>600**	99	1.4	<1
11	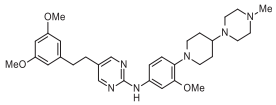	**1120**	**21**	**227**	324	15.1	≥100
20b	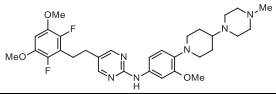	**1220**	**85**	**176**	13	18.4	79

[a] Plasma concentrations were measured using LC-MS/MS 6 h after single oral administration of test compounds at 30 mg/kg to ICR mice (average of 3 mice).
[b] *In vivo* inhibition rate of FGFR3 phosphorylation in nude mice xenografted with NIH/3T3 cells exogenously overexpressing FGFR3 S249C 6 h after single oral administration of test compounds at 30 mg/kg (average of 3 mice).
[c] *In vitro* intrinsic clearance in ICR mouse liver microsomes.
[d] NIH/3T3 cells exogenously overexpressing FGFR3 S249C.
[e] Parallel artificial membrane permeability assay (PAMPA) at pH = 6.5.
[f] Aqueous solubility in the Japanese Pharmacopoeia 2nd fluid for disintegration test (JP2: pH = 6.8 buffer).
[g] Not tested.

Table 6
In vitro pharmacological profiles of **20b**.

Enzyme IC_{50} (nM)					Cellular IC_{50} (nM)	
FGFR1	**FGFR2**	FGFR3	**FGFR4**	**VEGFR2**	**UM-UC-14**	NIH/3T3 (FGFR3 S249C)
1.7	**1.2**	1.2	**4.2**	**34**	**21**	13

Table 7
In vivo antitumor efficacy of once daily oral administration of **20b** for 11 days in a nude mouse model xenografted with UM-UC-14 bladder cancer cells (average of 5 mice).

Dose (mg/kg)	0.1	0.3	1	3	10[a]
Antitumor effect	1.4% inh.	48% inh.	62% inh.	42% reg.	75% reg.

[a] Body weight loss was observed.

approach to that described for **5a**. ^{1}H NMR (400 MHz, DMSO-d_6) δ ppm 1.47–1.61 (2H, m), 1.74–1.85 (2H, m), 2.14 (3H, s), 2.20–2.56 (11H, m), 3.00 (3H, br s), 3.28–3.39 (2H, m), 3.45–3.59 (2H, m), 3.77 (3H, s), 3.94–4.06 (2H, m), 6.87 (1H, d, J = 8.6 Hz), 7.27 (1H, d, J = 2.4 Hz), 7.31–7.40 (1H, m), 8.97 (1H, s), 9.05 (1H, br s), 10.27 (1H, br s); MS (ESI) m/z $[M + H]^+$ 549.

5.1.3. *N-{3-Methoxy-4-[4-(4-methylpiperazin-1-yl)piperidin-1-yl] phenyl}-5-nitropyrimidin-2-amine (**5c**)*

To a mixture of **4** (973 mg, 3.20 mmol) in EtOH (10.2 mL) was added MsOH (0.415 mL, 6.39 mmol). After stirring at room temperature for 20 min, 2-chloro-5-nitropyrimidine (**3c**, 510 mg, 3.20 mmol) was added to the mixture. After stirring at 100 °C for 4 h, the mixture was quenched with sat. $NaHCO_3$ *aq.* and extracted with $CHCl_3$. The organic layer was dried over Na_2SO_4 and concentrated *in vacuo*. The residue was purified by column chromatography on amino functionalized silica gel ($CHCl_3$/MeOH = 100:0 to 80:20) to give the product (858 mg, 63%) as a brown solid. ^{1}H NMR (400 MHz, $CDCl_3$) δ ppm 1.74–1.95 (4H, m), 2.30 (3H, s), 2.36–2.74 (11H, m), 3.46–3.59 (2H, m), 3.88–3.92 (3H, m), 6.91–6.97 (1H, m), 7.04–7.09 (1H, m), 7.23–7.29 (1H, m), 7.62 (1H, br s), 9.17 (2H, br s); MS (APCI/ESI) m/z $[M + H]^+$ 428.

5.1.4. *N^2-{3-Methoxy-4-[4-(4-methylpiperazin-1-yl)piperidin-1-yl] phenyl}-N^4-phenylpyrimidine-2,4,5-triamine (**6a**)*

To a mixture of **5a** (450 mg, 0.868 mmol) in EtOH (15.0 mL) and THF (25.0 mL) was added 10% Pd/C (50% wet, 110 mg). After stirring at room temperature under a hydrogen atmosphere (1.0 atm) for 3 h, the mixture was passed through a Celite pad. The filtrate was concentrated *in vacuo*. To the reaction mixture were added EtOH (12.0 mL), THF (12.0 mL) and 10% Pd/C (50% wet, 240 mg). After stirring at room temperature under a hydrogen atmosphere (1.0 atm) for 7 h, the mixture was passed through a Celite pad. The filtrate was concentrated *in vacuo* to give the product (506 mg, quantitative yield) as a grey solid. MS (ESI) m/z $[M + H]^+$ 489.

5.1.5. *N^4-[2-(Methanesulfonyl)ethyl]–N^2-{3-methoxy-4-[4-(4-methylpiperazin-1-yl)piperidin-1-yl]phenyl}pyrimidine-2,4,5-triamine (**6b**)*

To a mixture of **5b** (710 mg, 1.29 mmol) in EtOH (15.0 mL) and THF (30.0 mL) was added 10% Pd/C (50% wet, 331 mg). After stirring at room temperature under a hydrogen atmosphere (1.0 atm) for 7 h, the mixture was passed through a Celite pad. The filtrate was concentrated *in vacuo*. The residue was diluted with $CHCl_3$ and dried over $MgSO_4$ and concentrated *in vacuo*. The residue was purified by column chromatography on silica gel ($CHCl_3$/MeOH/28% NH_3 *aq.* = 100:0:0 to 90:9:1) to give the product (710 mg, quantitative yield) as a grey solid. ^{1}H NMR (399 MHz, DMSO-d_6) δ ppm 1.45–1.60 (2H, m), 1.72–1.85 (2H, m), 2.14 (3H, s), 2.19–2.57 (11H, m), 3.02 (3H, s), 3.22–3.34 (2H, m), 3.45 (2H, t, J = 6.7 Hz), 3.73 (3H, s), 3.76–3.85 (2H, m), 3.98 (2H, s), 6.62 (1H, t, J = 5.8 Hz), 6.74 (1H, d, J = 8.6 Hz), 7.24 (1H, dd, J = 8.6, 2.2 Hz), 7.30 (1H, d, J = 2.4 Hz), 7.42 (1H, s), 8.29 (1H, s); MS (ESI) m/z $[M + H]^+$ 519.

5.1.6. *N^2-{3-Methoxy-4-[4-(4-methylpiperazin-1-yl)piperidin-1-yl] phenyl}pyrimidine-2,5-diamine (**6c**)*

To a mixture of **5c** (858 mg, 2.01 mmol) in EtOH (15.0 mL) was added 10% Pd/C (55% wet, 107 mg). After stirring at room temperature under a hydrogen atmosphere (1.0 atm) for 12 h, the mixture was passed through a Celite pad. The filtrate was concentrated *in vacuo*. The residue was purified by column chromatography on silica gel ($CHCl_3$/MeOH = 100:0 to 80:20) to give the product (567 mg, 71%) as a brown solid. ^{1}H NMR (400 MHz, $CDCl_3$) δ ppm 1.73–1.93 (4H, m), 2.29 (3H, s), 2.34–2.74 (11H, m), 3.25 (2H, s), 3.40–3.56 (2H, m), 3.87 (3H, s), 6.72

(1H, s), 6.88 (1H, d, $J = 8.4$ Hz), 6.99 (1H, dd, $J = 8.4$, 2.2 Hz), 7.20 (1H, d, $J = 2.2$ Hz), 8.01 (2H, s); MS (APCI/ESI) *m/z* $[M + H]^+$ 398.

*5.1.7. N-(4-Anilino-2-{3-methoxy-4-[4-(4-methylpiperazin-1-yl)piperidin-1-yl]anilino}pyrimidin-5-yl)-3,5-dimethoxybenzamide (**7a**)*

To a mixture of **6a** (254 mg, 0.520 mmol) in THF (10.0 mL) were added DIPEA (98.3 μL, 0.574 mmol) and 3,5-dimethoxybenzoyl chloride (120 mg, 0.598 mmol). After stirring at room temperature for 3 h, the mixture was quenched with sat. $NaHCO_3$ *aq.* and extracted with $CHCl_3$. The organic layer was washed with brine, dried over $MgSO_4$ and concentrated *in vacuo*. The residue was purified by column chromatography on silica gel ($CHCl_3$/MeOH/28% NH_3 *aq.* = 100:0:0 to 90:9:1). EtOAc was added to the residue, and the resulting precipitate was filtered and dried to give the product (103 mg, 30%) as a grey solid. ^{1}H NMR (400 MHz, DMSO-d_6) δ ppm 1.48–1.59 (2H, m), 1.76–1.83 (2H, m), 2.15 (3H, s), 2.20–2.58 (11H, m), 3.26–3.37 (2H, m), 3.59 (3H, s), 3.82 (6H, s), 6.71–6.77 (2H, m), 7.02–7.07 (1H, m), 7.20–7.32 (6H, m), 7.63–7.72 (2H, m), 7.97 (1H, s), 8.59 (1H, s), 9.01 (1H, s), 9.57 (1H, s); MS (ESI) *m/z* $[M + H]^+$ 653; HRMS (ESI) *m/z* Calcd for $C_{36}H_{45}N_8O_4$ $[M + H]^+$: 653.3558. Found: 653.3548; *Anal.* Calcd for $C_{36}H_{44}N_8O_4.0.6H_2O$: C, 65.16; H, 6.87; N, 16.89. Found: C, 65.11; H, 6.94; N, 16.87.

*5.1.8. N-(4-{[2-(Methanesulfonyl)ethyl]amino}-2-{3-methoxy-4-[4-(4-methylpiperazin-1-yl)piperidin-1-yl]anilino}pyrimidin-5-yl)-3,5-dimethoxybenzamide (**7b**)*

A mixture of **6b** (200 mg, 0.386 mmol), 3,5-dimethoxybenzoic acid (84.3 mg, 0.463 mmol), DIPEA (132 μL, 0.771 mmol), and HATU (182 mg, 0.479 mmol) in DMF (4.00 mL) was stirred at room temperature overnight. The mixture was quenched with water and sat. $NaHCO_3$ *aq.* and extracted with EtOAc. The organic layer was washed with brine, dried over $MgSO_4$ and concentrated *in vacuo*. The residue was purified twice by column chromatography on silica gel ($CHCl_3$/MeOH/28% NH_3 *aq.* = 100:0:0 to 90:9:1). EtOAc/IPE was added to the residue, and the resulting precipitate was filtered and dried to give the product (86 mg, 33%) as a colorless solid. ^{1}H NMR (400 MHz, DMSO-d_6) δ ppm 1.45–1.62 (2H, m), 1.75–1.84 (2H, m), 2.14 (3H, s), 2.20–2.57 (11H, m), 3.01 (3H, s), 3.26–3.35 (2H, m), 3.42 (2H, t, $J = 6.8$ Hz), 3.74–3.84 (11H, m), 6.70 (1H, t, $J = 2.2$ Hz), 6.77–6.83 (1H, m), 6.93–7.02 (1H, m), 7.15 (2H, d, $J = 2.4$ Hz), 7.30–7.35 (2H, m), 7.77 (1H, s), 8.91 (1H, s), 9.47 (1H, s); MS (ESI) *m/z* $[M + H]^+$ 683; HRMS (ESI) *m/z* Calcd for $C_{33}H_{47}N_8O_6S$ $[M + H]^+$: 683.3334. Found: 683.3324; *Anal.* Calcd for $C_{33}H_{46}N_8O_6S.0.08IPE.1.7H_2O$: C, 55.72; H, 7.06; N, 15.53; S, 4.44. Found: C, 55.79; H, 6.91; N, 15.34; S, 4.39.

*5.1.9. 3,5-Dimethoxy-N-(2-{3-methoxy-4-[4-(4-methylpiperazin-1-yl)piperidin-1-yl]anilino}pyrimidin-5-yl)benzamide (**7c**)*

Compound **7c** was prepared from **6c** in 51% yield using a similar approach to that described for **7b**. ^{1}H NMR (400 MHz, DMSO-d_6) δ ppm 1.48–1.61 (2H, m), 1.75–1.85 (2H, m), 2.14–2.71 (14H, m), 3.25–3.37 (2H, m), 3.77 (3H, s), 3.83 (6H, s), 6.73 (1H, t, $J = 2.2$ Hz), 6.82 (1H, d, $J = 8.6$ Hz), 7.12 (2H, d, $J = 2.2$ Hz), 7.28 (1H, dd, $J = 8.5$, 2.3 Hz), 7.36 (1H, d, $J = 2.4$ Hz), 8.73 (2H, s), 9.38 (1H, s), 10.21 (1H, s); MS (ESI) *m/z* $[M + H]^+$ 562; HRMS (ESI) *m/z* Calcd for $C_{30}H_{40}N_7O_4$ $[M + H]^+$: 562.3136. Found: 562.3134; *Anal.* Calcd for $C_{30}H_{39}N_7O_4.0.14IPE.1.2H_2O$: C, 61.98; H, 7.31; N, 16.41. Found: C, 62.01; H, 7.45; N, 16.23.

*5.1.10. N^5-[(3,5-Dimethoxyphenyl)methyl]-N^2-{3-methoxy-4-[4-(4-methylpiperazin-1-yl)piperidin-1-yl]phenyl}pyrimidine-2,5-diamine (**7d**)*

To a mixture of **6c** (150 mg, 0.377 mmol) in CH_2Cl_2 (6.00 mL) were added 3,5-dimethoxybenzaldehyde (56.4 mg, 0.340 mmol) and NaBH$(OAc)_3$ (120 mg, 0.566 mmol). After stirring at room temperature overnight, the mixture was quenched with water and sat. $NaHCO_3$ *aq.* and extracted with $CHCl_3$. The organic layer was washed with brine, dried over $MgSO_4$ and concentrated *in vacuo*. The residue was purified twice by column chromatography on silica gel ($CHCl_3$/MeOH/28% NH_3 *aq.* = 100:0:0 to 90:9:1) to give the mixture.

To the mixture in MeOH (5.00 mL) was added $NaBH_4$ (57.1 mg, 1.51 mmol). After stirring at room temperature for 6 h, the mixture was quenched with water and sat. $NaHCO_3$ *aq.* and extracted with $CHCl_3$. The organic layer was washed with brine, dried over $MgSO_4$ and concentrated *in vacuo*. The residue was purified by column chromatography on silica gel ($CHCl_3$/MeOH/28% NH_3 *aq.* = 100:0:0 to 90:9:1). EtOAc/IPE was added to the residue, and the resulting precipitate was filtered and dried to give the product (33 mg, 16%) as an yellow solid. ^{1}H NMR (399 MHz, DMSO-d_6) δ ppm 1.43–1.61 (2H, m), 1.69–1.86 (2H, m), 2.14 (3H, s), 2.18–2.57 (11H, m), 3.21–3.36 (2H, m), 3.68–3.75 (9H, m), 4.19 (2H, d, $J = 6.3$ Hz), 5.89 (1H, t, $J = 6.3$ Hz), 6.36 (1H, t, $J = 2.2$ Hz), 6.55 (2H, d, $J = 2.4$ Hz), 6.74 (1H, d, $J = 8.6$ Hz), 7.18 (1H, dd, $J = 8.6$, 2.4 Hz), 7.29 (1H, d, $J = 2.4$ Hz), 7.92 (2H, s), 8.74 (1H, s); MS (ESI) *m/z* $[M + H]^+$ 548.

HRMS (ESI) *m/z* Calcd for $C_{30}H_{42}N_7O_3$ $[M + H]^+$: 548.3344. Found: 548.3341; *Anal.* Calcd for $C_{30}H_{41}N_7O_3.0.1EtOAc$: C, 65.6; H, 7.6; N, 17.6. Found: C, 65.5; H, 7.6; N, 17.5.

*5.1.11. 5-Bromo-N-{3-methoxy-4-[4-(4-methylpiperazin-1-yl)piperidin-1-yl]phenyl}pyrimidin-2-amine (**9**)*

To a mixture of 5-bromo-2-chloropyrimidine (**8**, 3.00 g, 15.5 mmol) and **4** (3.15 g, 10.3 mmol) in IPA (31.5 mL) was added MsOH (2.01 mL, 31.0 mmol). After stirring at 90 °C for 12 h and then 110 °C for 6 h, the mixture was quenched with $NaHCO_3$ *aq.* and extracted with $CHCl_3$. The organic layer was dried over Na_2SO_4 and concentrated *in vacuo*. The residue was purified by column chromatography on silica gel ($CHCl_3$/MeOH = 99:1 to 80:20) to give the product (3.76 g, 79%) as a pale yellow solid. ^{1}H NMR (400 MHz, $CDCl_3$) δ ppm 1.72–1.93 (4H, m), 2.29 (3H, s), 2.36–2.73 (11H, m), 3.45–3.56 (2H, m), 3.87 (3H, s), 6.90 (1H, d, $J = 8.4$ Hz), 7.00 (1H, dd, $J = 8.6$, 2.4 Hz), 7.09 (1H, s), 7.19 (1H, d, $J = 2.4$ Hz), 8.39 (2H, s); MS (APCI/ESI) *m/z* $[M + H]^+$ 461, 463.

*5.1.12. 5-[(3,5-Dimethoxyphenyl)ethynyl]-N-{3-methoxy-4-[4-(4-methylpiperazin-1-yl)piperidin-1-yl]phenyl}pyrimidin-2-amine (**10**)*

To a mixture of **9** (300 mg, 0.650 mmol), $Pd(PPh_3)_4$ (75.1 mg, 65.0 μmol), CuI (6.19 mg, 32.5 μmol), 1-ethynyl-3,5-dimethoxybenzene (316 mg, 1.95 mmol) in DMF (6.00 mL) was added Et_3N (223 μL, 1.30 mmol) under an argon atmosphere. After stirring at 110 °C for 4 h, the mixture was diluted with EtOAc and passed through a Celite pad. To the filtrate was added $NaHCO_3$ *aq.* and the mixture was extracted with EtOAc. The organic layer was washed with brine, dried over Na_2SO_4 and concentrated *in vacuo*. The residue was purified by column chromatography on silica gel ($CHCl_3$/MeOH = 100:0 to 80:20) to give crude material, which was purified again by column chromatography on amino functionalized silica gel (EtOAc/MeOH = 100:0 to 80:20) to give the product (328 mg, 93%) as an yellow solid. ^{1}H NMR (400 MHz, $CDCl_3$) δ ppm 1.73–1.96 (4H, m), 2.30 (3H, s), 2.36–2.74 (11H, m), 3.45–3.58 (2H, m), 3.81 (6H, s), 3.89 (3H, s), 6.47 (1H, t, $J = 2.3$ Hz), 6.67 (2H, d, $J = 2.3$ Hz), 6.92 (1H, d, $J = 8.6$ Hz), 7.04 (1H, dd, $J = 8.4$, 2.3 Hz), 7.09 (1H, br s), 7.23–7.28 (1H, m), 8.52 (2H, s); MS (APCI/ESI) *m/z* $[M + H]^+$ 543.

*5.1.13. 5-[2-(3,5-Dimethoxyphenyl)ethyl]-N-{3-methoxy-4-[4-(4-methylpiperazin-1-yl)piperidin-1-yl]phenyl}pyrimidin-2-amine (**11**)*

To a mixture of **10** (328 mg, 0.604 mmol) in MeOH (10.0 mL) and THF (10.0 mL) was added 10% Pd/C (50% wet, 64.0 mg) under an argon atmosphere. After stirring at room temperature under a hydrogen atmosphere (3.0 atm) for 3 h, 10% Pd/C (50% wet, 64.0 mg) was added to the mixture. After stirring at room temperature under a hydrogen atmosphere (3.0 atm) for 5 h, the mixture was passed through a Celite pad. The filtrate was concentrated *in vacuo*. The residue was purified by column chromatography on silica gel ($CHCl_3$/MeOH = 100:0 to 80:20), diluted with EtOAc and stirred under heating condition. After cooling to room temperature, the resulting precipitate was filtered and dried to give the product (180 mg, 54%) as a pale yellow solid. ^{1}H NMR (400

MHz, DMSO-d_6) δ ppm 1.46–1.59 (2H, m), 1.74–1.83 (2H, m), 2.14 (3H, s), 2.19–2.54 (11H, m), 2.71–2.82 (4H, m), 3.26–3.36 (2H, m), 3.70 (6H, s), 3.74 (3H, s), 6.30 (1H, t, J = 2.3 Hz), 6.38 (2H, d, J = 2.3 Hz), 6.79 (1H, d, J = 8.6 Hz), 7.24 (1H, dd, J = 8.6, 2.3 Hz), 7.35 (1H, d, J = 2.3 Hz), 8.26 (2H, s), 9.22 (1H, s); MS (ESI) m/z $[M + H]^+$ 547; HRMS (ESI) m/z Calcd for $C_{31}H_{43}N_6O_3$ $[M + H]^+$: 547.3391. Found: 547.3383; *Anal.* Calcd for $C_{31}H_{42}N_6O_3.0.4H_2O$: C, 67.22; H, 7.79; N, 15.17. Found: C, 67.40; H, 7.77; N, 15.00.

5.1.14. N-(2-Chloropyrimidin-5-yl)-3,5-dimethoxybenzamide (13a)

Compound **13a** was prepared from 2-chloropyrimidin-5-amine (**12a**) in 77% yield using a similar approach to that described for **7a**. ^{1}H NMR (400 MHz, DMSO-d_6) δ ppm 3.83 (6H, s), 6.78 (1H, t, J = 2.3 Hz), 7.14 (2H, d, J = 2.3 Hz), 9.13 (2H, s), 10.70 (1H, s); MS (ESI) m/z $[M + H]^+$ 294.

5.1.15. N-(2-Chloropyrimidin-5-yl)-3,5-dimethoxy-N-methylbenzamide (13b)

To a mixture of **13a** (690 mg, 2.35 mmol) in DMF (10.0 mL) was added NaH (113 mg, 2.58 mmol, 55% oil dispersion) in an ice-water bath. After stirring in an ice-water bath for 15 min, iodomethane (220 μL, 3.53 mmol) was added to the mixture. After stirring at room temperature for 4 h, the mixture was quenched with water in an ice-water bath and extracted with EtOAc. The organic layer was washed with brine, dried over $MgSO_4$ and concentrated *in vacuo*. The residue was purified by column chromatography on silica gel (*n*-hexane/EtOAc = 100:0 to 50:50) to give the product (530 mg, 73%) as an yellow solid. ^{1}H NMR (400 MHz, DMSO-d_6) δ ppm 3.38 (3H, s), 3.68 (6H, s), 6.48–6.53 (3H, m), 8.73 (2H, s); MS (APCI/ESI) m/z $[M + H]^+$ 308.

5.1.16. 2-Chloro-5-[(3,5-dimethoxyphenoxy)methyl]pyrimidine (13c)

To a mixture of (2-chloropyrimidin-5-yl)methanol (**12b**, 120 mg, 0.805 mmol) in THF (2.40 mL) were added 3,5-dimethoxyphenol (186 mg, 1.21 mmol), ADDP (305 mg, 1.21 mmol), and *n*-Bu_3P (244 mg, 1.21 mmol) in an ice-water bath. After stirring at room temperature for 12 h, the insoluble material was removed by filtration. The filtrate was concentrated *in vacuo* to give a residue, which was purified by column chromatography on silica gel (*n*-hexane/EtOAc = 90:10 to 0:100) to give the product (119 mg, 53%) as a colorless solid. ^{1}H NMR (400 MHz, $CDCl_3$) δ ppm 3.78 (6H, s), 5.03 (2H, s), 6.11–6.16 (3H, m), 8.70 (2H, s); MS (APCI/ESI) m/z $[M + H]^+$ 281.

5.1.17. 2-Chloro-5-[(3,5-dimethoxyphenyl)methoxy]pyrimidine (13d)

To a mixture of 2-chloropyrimidin-5-ol (**12c**, 278 mg, 2.13 mmol) in DMF (3.00 mL) were added K_2CO_3 (453 mg, 3.28 mmol) and 3,5-dimethoxybenzyl bromide (541 mg, 2.34 mmol) in an ice-water bath. After stirring at room temperature for 7 h, the mixture was quenched with water and sat. $NaHCO_3$ *aq.* and extracted with EtOAc. The organic layer was washed with brine, dried over $MgSO_4$ and concentrated *in vacuo*. The residue was purified by column chromatography on silica gel (*n*-hexane/EtOAc = 100:0 to 75:25) to give the product (360 mg, 60%) as a colorless solid. ^{1}H NMR (400 MHz, DMSO-d_6) δ ppm 3.75 (6H, s), 5.20 (2H, s), 6.48 (1H, t, J = 2.3 Hz), 6.63 (2H, d, J = 2.4 Hz), 8.60 (2H, s); MS (APCI/ESI) m/z $[M + H]^+$ 281.

5.1.18. 3,5-Dimethoxy-N-(2-{3-methoxy-4-[4-(4-methylpiperazin-1-yl) piperidin-1-yl]anilino}pyrimidin-5-yl)-N-methylbenzamide (14a)

To a mixture of **13b** (195 mg, 0.634 mmol), **4** (295 mg, 0.969 mmol), *rac*-BINAP (119 mg, 0.191 mmol), and Cs_2CO_3 (619 mg, 1.90 mmol) in 1,4-dioxane (8.00 mL) was added $Pd(OAc)_2$ (39.0 mg, 0.174 mmol). After stirring at 100 °C for 3 h, the mixture was quenched with water and extracted with EtOAc. The organic layer was washed with brine, dried over $MgSO_4$ and concentrated *in vacuo*. The residue was purified twice by column chromatography on silica gel ($CHCl_3$/MeOH/28% NH_3 *aq.* = 100:0:0 to 90:9:1). EtOAc/IPE was added to the residue, and the resulting precipitate was filtered and dried to give the product (153 mg, 42%) as a pale yellow solid. ^{1}H NMR (400 MHz, DMSO-d_6) δ ppm 1.45–1.60 (2H, m), 1.72–1.84 (2H, m), 2.14 (3H, s), 2.20–2.59 (11H, m), 3.22–3.39 (5H, m), 3.57–3.69 (6H, m), 3.73 (3H, s), 6.32–6.52 (3H, m), 6.79 (1H, d, J = 8.6 Hz), 7.16–7.29 (2H, m), 8.32 (2H, br s), 9.47 (1H, s); MS (ESI) m/z $[M + H]^+$ 576; HRMS (ESI) m/z Calcd for $C_{31}H_{42}N_7O_4$ $[M + H]^+$: 576.3293. Found: 576.3288; *Anal.* Calcd for $C_{31}H_{41}N_7O_4.0.3IPE.1.2H_2O$: C, 62.73; H, 7.64; N, 15.61. Found: C, 62.64; H, 7.40; N, 15.62.

5.1.19. 5-[(3,5-Dimethoxyphenoxy)methyl]-N-{3-methoxy-4-[4-(4-methylpiperazin-1-yl)piperidin-1-yl]phenyl}pyrimidin-2-amine (14b)

Compound **14b** was prepared from **13c** and **4** in 82% yield using a similar approach to that described for **14a**. ^{1}H NMR (400 MHz, DMSO-d_6) δ ppm 1.47–1.60 (2H, m), 1.76–1.83 (2H, m), 2.14 (3H, s), 2.19–2.58 (11H, m), 3.26–3.36 (2H, m), 3.71 (6H, s), 3.76 (3H, s), 4.94 (2H, s), 6.12 (1H, t, J = 2.2 Hz), 6.20 (2H, d, J = 2.2 Hz), 6.81 (1H, d, J = 8.6 Hz), 7.27 (1H, dd, J = 8.6, 2.4 Hz), 7.36 (1H, d, J = 2.4 Hz), 8.52 (2H, s), 9.50 (1H, s); MS (ESI) m/z $[M + H]^+$ 549; HRMS (ESI) m/z Calcd for $C_{30}H_{41}N_6O_4$ $[M + H]^+$: 549.3184. Found: 549.3182; *Anal.* Calcd for $C_{30}H_{40}N_6O_4.0.05EtOAc.0.04H_2O$: C, 65.50; H, 7.37; N, 15.18. Found: C, 65.49; H, 7.43; N, 15.05.

5.1.20. 5-[(3,5-Dimethoxyphenyl)methoxy]-N-{3-methoxy-4-[4-(4-methylpiperazin-1-yl)piperidin-1-yl]phenyl}pyrimidin-2-amine (14c)

Compound **14c** was prepared from **13d** and **4** in 33% yield using a similar approach to that described for **14a**. ^{1}H NMR (399 MHz, DMSO-d_6) δ ppm 1.43–1.62 (2H, m), 1.68–1.87 (2H, m), 2.14 (3H, s), 2.17–2.70 (11H, m), 3.23–3.35 (2H, m), 3.74 (6H, s), 3.74 (3H, s), 5.07 (2H, s), 6.46 (1H, t, J = 2.4 Hz), 6.60 (2H, d, J = 2.4 Hz), 6.78 (1H, d, J = 8.6 Hz), 7.23 (1H, dd, J = 8.6, 2.2 Hz), 7.32 (1H, d, J = 2.2 Hz), 8.29 (2H, s), 9.15 (1H, s); MS (ESI) m/z $[M + H]^+$ 549; HRMS (ESI) m/z Calcd for $C_{30}H_{41}N_6O_4$ $[M + H]^+$: 549.3184. Found: 549.3179; *Anal.* Calcd for $C_{30}H_{40}N_6O_4.0.01IPE.0.03H_2O$: C, 65.6; H, 7.4; N, 15.3. Found: C, 65.9; H, 7.4; N, 15.0.

5.1.21. 2,4-Dichloro-3-ethynyl-1,5-dimethoxybenzene (16a)

To a mixture of 1-ethynyl-3,5-dimethoxybenzene (**15**, 500 mg, 3.08 mmol) in MeCN (10.0 mL) was added SO_2Cl_2 (524 μL, 6.47 mmol) in an ice-water bath under an argon atmosphere. After stirring at room temperature for 12 h, the mixture was concentrated *in vacuo* to give a residue, which was purified by column chromatography on silica gel (*n*-hexane/EtOAc = 98:2 to 60:40) to give the product (335 mg, 47%) as a colorless solid. ^{1}H NMR (400 MHz, $CDCl_3$) δ ppm 3.68 (1H, s), 3.92 (6H, s), 6.58 (1H, s); MS (APCI/ESI) m/z $[M + H]^+$ 231.

5.1.22. 3-Ethynyl-2,4-difluoro-1,5-dimethoxybenzene (16b)

.

5.1.23. 1-Ethynyl-2-fluoro-3,5-dimethoxybenzene (16c)

To a mixture of **15** (5.00 g, 30.8 mmol) in MeCN (100 mL) was added Selectfluor™ (24.3 g, 61.7 mmol) in an ice-water bath. The mixture was allowed to gradually warm to room temperature and stirred for 4 days. The mixture was quenched with $NaHCO_3$ *aq.* and extracted with EtOAc. The organic layer was washed with brine, dried over Na_2SO_4 and concentrated *in vacuo*. The residue was purified by column chromatography on silica gel (*n*-hexane/EtOAc = 95:5 to 70:30) to give **16c** (1.74 g, 31%) as a pale yellow oil and crude material for **16b**, which was purified twice by column chromatography on silica gel (*n*-hexane/$CHCl_3$ = 50:50 to 0:100) to give **16b** (1.21 g, 20%) as a colorless solid. ^{1}H NMR (400 MHz, $CDCl_3$) δ ppm 3.52 (1H, s), 3.88 (6H, s), 6.66 (1H, t, J = 8.0 Hz); MS (EI) m/z $[M]^+$ 198 (for **16b**); ^{1}H NMR (400 MHz, $CDCl_3$) δ ppm 3.29 (1H, s), 3.77 (3H, s), 3.86 (3H, s), 6.49 (1H, dd, J = 4.5, 2.9 Hz), 6.54 (1H, dd, J = 7.0, 2.9 Hz); MS (APCI/ESI) m/z $[M + H]^+$ 181 (for **16c**).

*5.1.24. 2-Chloro-3-ethynyl-4-fluoro-1,5-dimethoxybenzene (**16d**)*

Compound **16d** was prepared from **16c** in 83% yield using a similar approach to that described for **16a**. ^{1}H NMR (400 MHz, $CDCl_3$) δ ppm 3.60 (1H, s), 3.89 (3H, s), 3.91 (3H, s), 6.61 (1H, d, J = 7.5 Hz); MS (CI) m/z $[M]^+$ 214.

*5.1.25. 5-Iodo-N-{3-methoxy-4-[4-(4-methylpiperazin-1-yl)piperidin-1-yl]phenyl}pyrimidin-2-amine (**18**)*

To a mixture of 2-chloro-5-iodopyrimidine (**17**, 1.00 g, 4.16 mmol) and **4** (1.27 g, 4.16 mmol) in IPA (20.0 mL) was added MsOH (809 μL, 12.5 mmol). After stirring at 130 °C for 3 h under μW irradiation, the mixture was quenched with $NaHCO_3$ *aq.* and extracted with $CHCl_3$. The organic layer was dried over Na_2SO_4 and concentrated *in vacuo*. The residue was purified by column chromatography on silica gel ($CHCl_3$/MeOH = 100:0 to 80:20) to give the crude product, which was purified again by column chromatography on amino functionalized silica gel (EtOAc/MeOH = 100:0 to 80:20). EtOAc was added to the residue, and the resulting precipitate was filtered and dried to give the product (1.76 g, 83%) as a pale yellow solid. ^{1}H NMR (400 MHz, $CDCl_3$) δ ppm 1.74–1.98 (4H, m), 2.25–2.34 (3H, m), 2.36–2.72 (11H, m), 3.46–3.55 (2H, m), 3.85–3.89 (3H, m), 6.86–6.94 (1H, m), 6.94–7.01 (2H, m), 7.16–7.21 (1H, m), 8.49 (2H, s); MS (APCI/ESI) m/z $[M + H]^+$ 509.

*5.1.26. 5-[(2,6-Dichloro-3,5-dimethoxyphenyl)ethynyl]-N-{3-methoxy-4-[4-(4-methylpiperazin-1-yl)piperidin-1-yl]phenyl}pyrimidin-2-amine (**19a**)*

To a mixture of **18** (200 mg, 0.393 mmol), **16a** (100 mg, 0.433 mmol), $Pd(PPh_3)_4$ (22.7 mg, 19.7 μmol), CuI (3.75 mg, 19.7 μmol) in DMF (4.00 mL) was added DIPEA (135 μL, 0.787 mmol) under an argon atmosphere. After stirring at 80 °C for 1 h, the mixture was diluted with EtOAc and water and passed through a Celite pad. The organic layer was separated and washed with brine, dried over Na_2SO_4 and concentrated *in vacuo*. The residue was purified by column chromatography on silica gel ($CHCl_3$/MeOH = 100:0 to 80:20) to give the product (126 mg, 52%) as a pale yellow solid. ^{1}H NMR (400 MHz, $CDCl_3$) δ ppm 1.74–1.94 (4H, m), 2.30 (3H, s), 2.37–2.75 (11H, m), 3.47–3.56 (2H, m), 3.89 (3H, s), 3.94 (6H, s), 6.57 (1H, s), 6.91 (1H, d, J = 8.6 Hz), 6.99–7.05 (1H, m), 7.16 (1H, s), 7.31 (1H, d, J = 2.4 Hz), 8.60 (2H, s); MS (APCI/ESI) m/z $[M + H]^+$ 611, 613.

*5.1.27. 5-[(2,6-Difluoro-3,5-dimethoxyphenyl)ethynyl]-N-{3-methoxy-4-[4-(4-methylpiperazin-1-yl)piperidin-1-yl]phenyl}pyrimidin-2-amine (**19b**)*

To a mixture of **18** (182 mg, 0.358 mmol), **16b** (85.1 mg, 0.430 mmol), $Pd(PPh_3)_4$ (41.4 mg, 35.8 μmol), CuI (3.41 mg, 17.9 μmol) in DMF (3.64 mL) was added Et_3N (123 μL, 0.716 mmol) under an argon atmosphere. After stirring at 100 °C for 4 h, the mixture was diluted with EtOAc and passed through a Celite pad. The filtrate was diluted with $NaHCO_3$ *aq.* and extracted with EtOAc. The organic layer was washed with brine, dried over Na_2SO_4 and concentrated *in vacuo*. The residue was purified by column chromatography on silica gel ($CHCl_3$/MeOH = 100:0 to 80:20) to give crude material, which was purified again by column chromatography on amino functionalized silica gel (EtOAc/MeOH = 100:0 to 80:20). The residue was added EtOAc and stirred under heating condition. After cooling to room temperature, the resulting precipitate was filtered and dried to give the product (120 mg, 58%) as an yellow solid. ^{1}H NMR (400 MHz, DMSO-d_6) δ ppm 1.44–1.68 (2H, m), 1.71–1.91 (2H, m), 2.17–2.75 (14H, m), 3.24–3.41 (2H, m), 3.77 (3H, s), 3.90 (6H, s), 6.84 (1H, d, J = 8.6 Hz), 7.10 (1H, t, J = 8.4 Hz), 7.27 (1H, dd, J = 8.6, 2.4 Hz), 7.33 (1H, d, J = 2.4 Hz), 8.64 (2H, s), 9.91 (1H, s); MS (ESI) m/z $[M + H]^+$ 579.

*5.1.28. 5-[(2-Fluoro-3,5-dimethoxyphenyl)ethynyl]-N-{3-methoxy-4-[4-(4-methylpiperazin-1-yl)piperidin-1-yl]phenyl}pyrimidin-2-amine (**19c**)*

Compound **19c** was prepared from **18** and **16c** in 55% yield using a similar approach to that described for **19a**. ^{1}H NMR (399 MHz, DMSO-d_6) δ ppm 1.43–1.64 (2H, m), 1.71–1.88 (2H, m), 2.14 (3H, s), 2.20–2.59 (11H, m), 3.26–3.39 (2H, m), 3.74–3.80 (6H, m), 3.85 (3H, s), 6.65 (1H, dd, J = 4.7, 2.9 Hz), 6.79 (1H, dd, J = 7.0, 2.9 Hz), 6.84 (1H, d, J = 8.6 Hz), 7.27 (1H, dd, J = 8.6, 2.4 Hz), 7.32 (1H, d, J = 2.4 Hz), 8.62 (2H, s), 9.84 (1H, s); MS (ESI) m/z $[M + H]^+$ 561.

*5.1.29. 5-[(2-Chloro-6-fluoro-3,5-dimethoxyphenyl)ethynyl]-N-{3-methoxy-4-[4-(4-methylpiperazin-1-yl)piperidin-1-yl]phenyl}pyrimidin-2-amine (**19d**)*

Compound **19d** was prepared from **18** and **16d** in 66% yield using a similar approach to that described for **19a**. ^{1}H NMR (399 MHz, DMSO-d_6) δ ppm 1.46–1.62 (2H, m), 1.71–1.88 (2H, m), 2.14 (3H, s), 2.20–2.58 (11H, m), 3.28–3.38 (2H, m), 3.77 (3H, s), 3.89–3.97 (6H, m), 6.84 (1H, d, J = 8.6 Hz), 7.04 (1H, d, J = 8.0 Hz), 7.26 (1H, dd, J = 8.6, 2.2 Hz), 7.35 (1H, d, J = 2.4 Hz), 8.64 (2H, s), 9.91 (1H, s); MS (ESI) m/z $[M + H]^+$ 595.

*5.1.30. 5-[2-(2,6-Dichloro-3,5-dimethoxyphenyl)ethyl]-N-{3-methoxy-4-[4-(4-methylpiperazin-1-yl)piperidin-1-yl]phenyl}pyrimidin-2-amine (**20a**)*

A mixture of **19a** (126 mg, 0.206 mmol) and *p*-toluenesulfonyl hydrazide (1.92 g, 10.3 mmol) in DME (2.52 mL) was stirred at 110 °C. To the mixture was added a solution of NaOAc (845 mg, 10.3 mmol) in water (2.52 mL) over 2 h. After stirring at 110 °C for 2 h, *p*-toluenesulfonyl hydrazide (1.92 g, 10.3 mmol) and NaOAc (845 mg, 10.3 mmol) were added over 2 h. After stirring at 110 °C for 2 h, the mixture was neutralized with $NaHCO_3$ *aq.* and extracted with $CHCl_3$. The organic layer was dried over Na_2SO_4 and concentrated *in vacuo*. A mixture of the residue and *p*-toluenesulfonyl hydrazide (1.92 g, 10.3 mmol) in DME (2.52 mL) was stirred at 110 °C. To the mixture was added a solution of NaOAc (845 mg, 10.3 mmol) in water (2.52 mL) over 2 h. After stirring at 110 °C for 2 h, the mixture was neutralized with $NaHCO_3$ *aq.* and extracted with $CHCl_3$. The organic layer was dried over Na_2SO_4 and concentrated *in vacuo*. The residue was purified by column chromatography on silica gel ($CHCl_3$/MeOH/28% NH_3 *aq.* = 100:0:0 to 80:18:2). EtOAc was added to the residue, and the resulting precipitate was filtered, washed with IPE, and dried to give the product (53.0 mg, 42%) as a pale yellow solid. ^{1}H NMR (400 MHz, DMSO-d_6) δ ppm 1.46–1.60 (2H, m), 1.74–1.83 (2H, m), 2.14 (3H, s), 2.20–2.56 (11H, m), 2.65–2.72 (2H, m), 3.08–3.17 (2H, m), 3.26–3.35 (2H, m), 3.75 (3H, s), 3.90 (6H, s), 6.79 (1H, d, J = 8.8 Hz), 6.83 (1H, s), 7.24 (1H, dd, J = 8.6, 2.4 Hz), 7.37 (1H, d, J = 2.4 Hz), 8.23 (2H, s), 9.28 (1H, s); MS (ESI) m/z $[M + H]^+$ 615, 617; HRMS (ESI) m/z Calcd for $C_{31}H_{41}Cl_2N_6O_3$ $[M + H]^+$: 615.2612. Found: 615.2608; *Anal.* Calcd for $C_{31}H_{40}Cl_2N_6O_3$.0.2EtOAc.0.2H_2O: C, 59.98; H, 6.65; N, 13.20; Cl, 11.13. Found: C, 59.95; H, 6.52; N, 13.04; Cl, 11.27.

*5.1.31. 5-[2-(2,6-Difluoro-3,5-dimethoxyphenyl)ethyl]-N-{3-methoxy-4-[4-(4-methylpiperazin-1-yl)piperidin-1-yl]phenyl}pyrimidin-2-amine (**20b**)*

A mixture of **19b** (7.50 g, 13.0 mmol) and *p*-toluenesulfonyl hydrazide (24.2 g, 130 mmol) in DME (75.0 mL) was stirred at 110 °C. To the mixture was added a solution of NaOAc (10.6 g, 130 mmol) in water (15.0 mL) over 2 h. After stirring at 110 °C for 2 h, *p*-toluenesulfonyl hydrazide (12.1 g, 64.8 mmol) and NaOAc (5.32 g, 64.8 mmol) were added over 2 h. After stirring at 110 °C for 2 h, *p*-toluenesulfonyl hydrazide (12.1 g, 64.8 mmol) and NaOAc (5.32 g, 64.8 mmol) were added over 2 h. The mixture was stirred at 110 °C for 2 h. The mixture was neutralized with $NaHCO_3$ *aq.* and extracted with $CHCl_3$. The organic layer was dried over $MgSO_4$ and concentrated *in vacuo*. A mixture of the residue and *p*-toluenesulfonyl hydrazide (12.1 g, 64.8 mmol) in DME (75.0 mL) was stirred at 110 °C. To the mixture was added a solution of NaOAc (5.32 g, 64.8 mmol) in water (15.0 mL) over 2 h. After stirring at 110 °C for 2 h, *p*-toluenesulfonyl hydrazide (12.1 g, 64.8 mmol) and NaOAc (5.32 g, 64.8 mmol) were added over 2 h. After stirring at 110 °C for 2 h, the mixture was neutralized with $NaHCO_3$ *aq.* and extracted with $CHCl_3$. The organic layer was dried over $MgSO_4$ and concentrated *in vacuo*. The residue was purified by column chromatography on silica gel ($CHCl_3$/MeOH/28% NH_3 *aq.* = 100:0:0 to 80:18:2). EtOAc (140 mL) and EtOH (10 mL) were added to the residue, and the resulting precipitate

was filtered to give the crude product. EtOH (50 mL) was added to the crude product, and the resulting precipitate was filtered and dried to give the product (1.78 g, 24%) as a pale yellow solid. ^{1}H NMR (399 MHz, DMSO-d_6) δ ppm 1.46–1.59 (2H, m), 1.74–1.82 (2H, m), 2.14 (3H, s), 2.18–2.58 (11H, m), 2.65–2.75 (2H, m), 2.84–2.93 (2H, m), 3.24–3.38 (2H, m), 3.74 (3H, s), 3.81 (6H, s), 6.79 (1H, d, J = 8.8 Hz), 6.85 (1H, t, J = 8.4 Hz), 7.23 (1H, dd, J = 8.8, 2.4 Hz), 7.34 (1H, d, J = 2.4 Hz), 8.17 (2H, s), 9.25 (1H, s); MS (ESI) m/z $[M + H]^+$ 583; HRMS (ESI) m/z Calcd for $C_{31}H_{41}F_2N_6O_3$ $[M + H]^+$: 583.3203. Found: 583.3195; *Anal.* Calcd for $C_{31}H_{40}F_2N_6O_3.0.1H_2O$: C, 63.7; H, 6.9; N, 14.4; F, 6.5. Found: C, 63.8; H, 7.1; N, 14.2; F, 6.1.

5.1.32. 5-[2-(2-Fluoro-3,5-dimethoxyphenyl)ethyl]-N-{3-methoxy-4-[4-(4-methylpiperazin-1-yl)piperidin-1-yl]phenyl}pyrimidin-2-amine (20c)

A mixture of **19c** (122 mg, 0.218 mmol) and *p*-toluenesulfonyl hydrazide (2.03 g, 10.9 mmol) in DME (2.44 mL) was stirred at 110 °C. To the mixture was added a solution of NaOAc (893 mg, 10.9 mmol) in water (1.22 mL) over 2 h. After stirring at 110 °C for 2 h, *p*-toluenesulfonyl hydrazide (1.01 g, 5.45 mmol) and NaOAc (447 mg, 5.45 mmol) were added over 2 h. After stirring at 110 °C for 2 h, the mixture was neutralized with $NaHCO_3$ *aq.* and extracted with $CHCl_3$. The organic layer was dried over $MgSO_4$ and concentrated *in vacuo*. The residue was purified by column chromatography on amino functionalized silica gel (EtOAc/MeOH/28% NH_3 *aq.* = 100:0:0 to 80:18:2). EtOAc/IPE was added to the residue, and the resulting precipitate was filtered and dried to give the product (63.0 mg, 51%) as a pale yellow solid. ^{1}H NMR (399 MHz, DMSO-d_6) δ ppm 1.45–1.61 (2H, m), 1.73–1.83 (2H, m), 2.14 (3H, s), 2.19–2.56 (11H, m), 2.70–2.77 (2H, m), 2.79–2.87 (2H, m), 3.25–3.34 (2H, m), 3.70 (3H, s), 3.74 (3H, s), 3.78 (3H, s), 6.37 (1H, dd, J = 5.1, 2.9 Hz), 6.55 (1H, dd, J = 7.0, 2.9 Hz), 6.79 (1H, d, J = 8.6 Hz), 7.24 (1H, dd, J = 8.6, 2.4 Hz), 7.35 (1H, d, J = 2.2 Hz), 8.23 (2H, s), 9.24 (1H, s); MS (ESI) m/z $[M + H]^+$ 565; HRMS (ESI) m/z Calcd for $C_{31}H_{42}FN_6O_3$ $[M + H]^+$: 565.3297. Found: 565.3287; *Anal.* Calcd for $C_{31}H_{41}FN_6O_3.0.4H_2O$: C, 65.10; H, 7.37; N, 14.70; F, 3.32. Found: C, 65.18; H, 7.24; N, 14.55; F, 3.33.

5.1.33. 5-[2-(2-Chloro-6-fluoro-3,5-dimethoxyphenyl)ethyl]-N-{3-methoxy-4-[4-(4-methylpiperazin-1-yl)piperidin-1-yl]phenyl}pyrimidin-2-amine (20d)

A mixture of **19d** (126 mg, 0.212 mmol) and *p*-toluenesulfonyl hydrazide (1.97 g, 10.6 mmol) in DME (2.52 mL) was stirred at 110 °C. To the mixture was added a solution of NaOAc (870 mg, 10.6 mmol) in water (2.52 mL) over 2 h. After stirring at 110 °C for 2 h, *p*-toluenesulfonyl hydrazide (1.97 g, 10.6 mmol) and NaOAc (870 mg, 10.6 mmol) were added over 2 h. After stirring at 110 °C for 2 h, the mixture was neutralized with $NaHCO_3$ *aq.* and extracted with $CHCl_3$. The organic layer was dried over Na_2SO_4 and concentrated *in vacuo*. The residue was purified by column chromatography on silica gel ($CHCl_3$/MeOH/28% NH_3 *aq.* = 100:0:0 to 80:18:2) to give crude material, which was purified again by column chromatography on amino functionalized silica gel (EtOAc/MeOH/28% NH_3 *aq.* = 100:0:0 to 80:18:2). EtOAc/IPE was added to the residue, and the resulting precipitate was filtered and dried to give the product (88.0 mg, 69%) as a pale yellow solid. ^{1}H NMR (400 MHz, DMSO-d_6) δ ppm 1.47–1.61 (2H, m), 1.73–1.85 (2H, m), 2.17 (3H, s), 2.21–2.60 (11H, m), 2.65–2.75 (2H, m), 2.93–3.03 (2H, m), 3.24–3.39 (2H, m), 3.74 (3H, s), 3.84–3.88 (6H, m), 6.79 (1H, d, J = 8.6 Hz), 6.84 (1H, d, J = 7.8 Hz), 7.23 (1H, dd, J = 8.6, 2.4 Hz), 7.35 (1H, d, J = 2.4 Hz), 8.18 (2H, s), 9.26 (1H, s); MS (ESI) m/z $[M + H]^+$ 599; HRMS (ESI) m/z Calcd for $C_{31}H_{41}ClFN_6O_3$ $[M + H]^+$: 599.2907. Found: 599.2897; *Anal.* Calcd for $C_{31}H_{40}ClFN_6O_3.0.4H_2O$: C, 61.41; H, 6.78; N, 13.86; Cl, 5.85; F, 3.13. Found: C, 61.39; H, 6.78; N, 13.70; Cl, 5.91; F, 3.10.

5.2. Molecular modeling

Docking models of **11**, **20a**, and **20b** with FGFR3 were prepared by MOE[36] using the crystal structure of FGFR3 in complex with **11** (PDB code: 7DHL) as a template. Molecular dynamics simulations for the complexes were performed using GROMACS[37] ver. 2016.1 with the AMBER 99SB-ILDN force field for proteins and the general amber force field (GAFF) for ligands.

5.3. In vitro kinase inhibitory assay

Inhibitory activity of compounds against FGFR1, 2, 3, and 4, and VEGFR2 were evaluated using an off-chip mobility shift assay. FGFR1, 2, 3, and 4, and VEGFR2 kinase (Carna Bioscience, Kobe, Japan) and test compounds were incubated for 30 or 120 min at room temperature (RT). After the incubation, substrate and adenosine triphosphate (ATP) at 75 μmol/L for VEGFR2, FGFR2, and FGFR3, 125 μmol/L for FGFR1, and 300 μmol/L for FGFR4 were added and the reactions were incubated for 30 min at RT. The kinase reaction was stopped by the addition of termination buffer. The reaction mixtures were measured using an EZ Reader II (Perkin Elmer). Wells without ATP were measured as positive control (100% inhibition), and wells treated with DMSO were measured as a negative control (0% inhibition). The IC_{50} value of each experiment was calculated using Sigmoid-Emax non-linear regression analysis.

5.4. In vitro cell growth inhibition assay

NIH/3T3 cells exogenously overexpressing FGFR3 S249C were seeded in 96-well plates at 3000 cells per well and incubated overnight. The following day, the cells were exposed to test compounds for 5 days. Cell viability was measured using CellTiter-Glo (Promega, Madison, WI, USA). Data are presented as mean values from a single experiment performed in duplicate.

UM-UC-14 cells were purchased from ECACC (Salisbury, UK). The cells were cultured according to instructions from the supplier. The cells were seeded in 384-well plates at 900 cells per well and incubated overnight. The following day, the cells were exposed to **20b** for 5 days. Cell viability was measured using CellTiter-Glo (Promega, Madison, WI, USA). Data are presented as mean values from a single experiment performed in duplicate.

5.5. In vitro metabolic stability

To estimate the intrinsic clearance of compounds against mouse hepatic CYPs, test compounds (0.2 μM) were incubated with pooled mouse liver microsomes (0.2 mg protein/mL), NADPH (1 mM) and EDTA (0.1 mM) in pH 7.4 Na^+-K^+ phosphate buffer (100 mM) at 37 °C. Incubations were conducted for 0, 15, 30, and 45 min. The peak area of the compounds and internal standard was measured using liquid chromatography-tandem mass spectrometry (LC-MS/MS) and analyzed to calculate CL_{int} (mL/min/kg). Values are shown as an average of duplicate experiments.

5.6. Permeability

Parallel artificial membrane permeability assay (PAMPA) was conducted using STARlet 8ch (Hamilton Robotics, Reno, NV). In this assay, a 'sandwich' is formed by a 96-well microtiter plate (pION Inc., Billerica, MA) and a 96-well filter plate (pION Inc.) such that each composite well is divided into two chambers, with the donor at the bottom and acceptor at the top, separated by a lipid (pION Inc.)-coated microfilter disc. DMSO stock solutions (10 mM) of the test compounds were added to a mixture of aqueous buffer (pH 6.5) and DMSO (9:1). The drug solutions were filtered through a 96-well filter plate (PVDF, Corning Inc., Corning, NY) and added to the donor compartments. The plates were sandwiched together and acceptor buffer (pH 7.4, pION Inc.) was added to the acceptor compartment. The sandwiched plates were incubated at room temperature for 2 h under saturated water vapor conditions. After incubation, the amount of test compounds in the donor and acceptor

compartments was assayed using high performance liquid chromatography (HPLC). Permeability was calculated using PAMPA Evolution software (pION Inc.).

5.7. Aqueous solubility

Solubility of the test compounds was evaluated using the Japanese Pharmacopoeia 2nd fluid for disintegration test (JP2; pH = 6.8 buffer). DMSO stock solutions (10 mM) of the test compounds were prepared and added to JP2. The solutions were shaken at 1000 rpm at 25 °C under light-protected conditions for 20 h. Precipitates were filtered through a PVDF membrane filter (pore size 0.22 μm, MERCK) and the concentration (μM) of the compound in the filtrate was assayed using HPLC.

5.8. Animal experiments

All animal experimental procedures were approved by the Institutional Animal Care and Use Committee of Astellas Pharma Inc. Furthermore, Astellas Pharma Inc. Tsukuba Research Center was awarded Accreditation Status by the AAALAC International. All efforts were made to minimize the number of animals used and to avoid suffering and distress.

5.8.1. In vivo auto-phosphorylation inhibition assay

NIH/3T3 cells exogenously overexpressing FGFR3 S249C were subcutaneously inoculated into the flank of male Balb/c nude mice (Charles River Japan, Inc.). Test compounds (30 mg/kg) were suspended in vehicle (0.5% methylcellulose solution) and administered to mice by oral gavage. Tumor samples were collected from mice 6 h after a single dose of the test compounds. Frozen tumor samples were lysed, and phosphorylated and total FGFR3 levels were measured using a sandwich ELISA assay. The data are shown as an average of 3 mice.

5.8.2. In vivo antitumor assay

UM-UC-14 human bladder cancer cells were subcutaneously inoculated into the flank of male Balb/c nude mice (Charles River Japan, Inc.). Compound **20b** (0.1–10 mg/kg) was suspended in vehicle (0.5% methylcellulose solution) and orally administered to mice once daily from Day 1 to Day 11. Tumor volume was determined by calculating length × width^2 × 0.5. The data are shown as an average of 5 mice.

5.8.3. Mouse plasma concentration

Test compounds (30 mg/kg) were suspended in vehicle (0.5% methylcellulose solution) and orally administered to ICR mice (male, fasted). The plasma concentrations of test compounds were measured using LC-MS/MS 6 h after a single dose. The data are shown as an average of 3 mice.

Declaration of Competing Interest

The authors declare the following financial interests/personal relationships which may be considered as potential competing interests: [Ikumi Kuriwaki, Minoru Kameda, Kazuhiko Iikubo, Hiroyuki Hisamichi, Yuichiro Kawamoto, Hiroyuki Moritomo, Yoshinori Iwai, Atsushi Noda, Hiroshi Tomiyama are inventors of the following patent: WO 2013/129369 (A1). This research is a collaboration between Astellas Pharma Inc. and Kotobuki Pharmaceutical Co., Ltd. Ikumi Kuriwaki, Minoru Kameda, Kazuhiko Iikubo, Hiroyuki Moritomo, Yasushi Amano, Yukihiro Tateishi, Yuka Echizen, Taisuke Nakazawa, Masaaki Hirano are employees of Astellas Pharma Inc.; Yoshinori Iwai and Atsushi Noda are employees of Kotobuki Pharmaceutical Co., Ltd.; and Hiroshi Tomiyama is President and CEO of Kotobuki Pharmaceutical Co., Ltd., as of the date of manuscript submission].

Acknowledgements

The authors thank Dr. Susumu Watanuki for his valuable advice in the preparation of this manuscript; Drs. Tomoyuki Suzuki, Aya Kikuchi, Masateru Iizuka, and Ms. Ayako Nakayama for their contributions to the biological studies; Drs. Akihiro Yamada, Yoichi Naritomi, Toshiko Yahata, Yoshiteru Kamiyama, and Fumihiko Ushigome for their contributions to the pharmacokinetic studies; Mr. Noritaka Hamada and Dr. Kouji Yamazaki for their contribution to physicochemical studies; Drs. Kazuki Ono and Yohsuke Hagiwara for their contributions to molecular modeling; and the staff of the Division of Analytical Science Laboratories and Astellas Research Technologies Co., Ltd. for conducting screening studies for metabolic clearance, permeability, solubility, partition coefficient, elemental analysis, and spectral measurements.

Funding

This study was funded by Astellas Pharma Inc. and Kotobuki Pharmaceutical Co., Ltd.

References

1 Bedard PL, Hyman DM, Davids MS, Siu LL. Small molecules, big impact: 20 years of targeted therapy in oncology. *Lancet*. 2020;395:1078–1088.
2 Roskoski RJ. Properties of FDA-approved small molecule protein kinase inhibitors: A 2020 update. *Pharmacol Res*. 2020;152:104609.
3 Turner N, Grose R. Fibroblast growth factor signaling: from development to cancer. *Nat Rev Cancer*. 2010;10:116–129.
4 Tomlinson DC, Baldo O, Harnden P, Knowles MA. FGFR3 protein expression and its relationship to mutation status and prognostic variables in bladder cancer. *J Pathol*. 2007;213:91–98.
5 Guancial EA, Werner L, Bellmunt J, et al. FGFR3 expression in primary and metastatic urothelial carcinoma of the bladder. *Cancer Med*. 2014;3:835–844.
6 Williams SV, Hurst CD, Knowles MA. Oncogenic FGFR3 gene fusions in bladder cancer. *Hum Mol Genet*. 2013;22:795–803.
7 Nakanishi Y, Akiyama N, Tsukaguchi T, et al. Mechanism of oncogenic signal activation by the novel fusion kinase FGFR3-BAIAP2L1. *Mol Cancer Ther*. 2015;14:704–712.
8 The Cancer Genome Atlas Research Network. Comprehensive molecular characterization of urothelial bladder carcinoma. *Nature*. 2014;507:315–322.
9 Katoh M. Fibroblast growth factor receptors as treatment targets in clinical oncology. *Nat Rev Clin Oncol*. 2019;16:105–122.
10 Dai S, Zhou Z, Chen Z, Xu G, Chen Y. Fibroblast growth factor receptors (FGFRs): structures and small molecule inhibitors. *Cells*. 2019;8:614.
11 Liu F-T, Li N-G, Zhang Y-M, et al. Recent advance in the development of novel, selective and potent FGFR inhibitors. *Eur J Med Chem*. 2020;186:111884.
12 Gavine PR, Mooney L, Kilgour E, et al. AZD4547: an orally bioavailable, potent, and selective inhibitor of the fibroblast growth factor receptor tyrosine kinase family. *Cancer Res*. 2012;72:2045–2056.
13 Guagnano V, Furet P, Spanka C, et al. Discovery of 3-(2,6-dichloro-3,5-dimethoxy-phenyl)-1-{6-[4-(4-ethyl-piperazin-1-yl)-phenylamino]-pyrimidin-4-yl}-1-methyl-urea (NVP-BGJ398), a potent and selective inhibitor of the fibroblast growth factor receptor family of receptor tyrosine kinase. *J Med Chem*. 2011;54:7066–7083.
14 Hall TG, Yu Y, Eathiraj S, et al. Preclinical activity of ARQ 087, a novel inhibitor targeting FGFR dysregulation. *PloS ONE*. 2016;11:e0162594.
15 Liu PCC, Koblish H, Wu L, et al. INCB054828 (pemigatinib), a potent and selective inhibitor of fibroblast growth factor receptors 1, 2, and 3, displays activity against genetically defined tumor models. *PLoS ONE*. 2020;15:e0231877.
16 Watanabe Miyano S, Yamamoto Y, Kodama K, et al. E7090, a novel selective inhibitor of fibroblast growth factor receptors, displays potent antitumor activity and prolongs survival in preclinical models. *Mol Cancer Ther*. 2016;15:2630–2639.
17 Nakanishi Y, Akiyama N, Tsukaguchi T, et al. The fibroblast growth factor receptor genetic status as a potential predictor of the sensitivity to CH5183284/Debio 1347, a novel selective FGFR inhibitor. *Mol Cancer Ther*. 2014;13:2547–2558.
18 Perera TPS, Jovcheva E, Mevellec L, et al. Discovery and pharmacological characterization of JNJ-42756493 (erdafitinib), a functionally selective small-molecule FGFR family inhibitor. *Mol Cancer Ther*. 2017;16:1010–1020.
19 Collin M-P, Lobell M, Hübsch W, et al. Discovery of rogaratinib (BAY 1163877): a pan-FGFR inhibitor. *Chem Med Chem*. 2018;13:437–445.
20 Brameld KA, Owens TD, Verner E, et al. Discovery of the irreversible covalent FGFR inhibitor 8-(3-(4-acryloylpiperazin-1-yl)propyl)-6-(2,6-dichloro-3,5-dimethoxyphenyl)-2-(methylamino)pyrido[2,3-*d*]pyrimidin-7(8*H*)-one (PRN1371) for the treatment of solid tumors. *J Med Chem*. 2017;60:6516–6527.
21 Kalyukina M, Yosaatmadja Y, Middleditch MJ, Patterson AV, Smaill JB, Squire CJ. TAS-120 cancer target binding: defining reactivity and revealing the first fibroblast growth factor receptor 1 (FGFR1) irreversible structure. *Chem Med Chem*. 2019;14:494–500.
22 Siefker-Radtke AO, Necchi A, Park SH, et al. First results from the primary analysis population of the phase 2 study of erdafitinib (JNJ-42756493) in patients with

metastatic or surgically unresectable urothelial carcinoma and FGFR alterations. Abstract# 4503 *ASCO Annual Meeting*. 2018:4503.
23 Johnson & Johnson Home Page. BALVERSA™ (erdafitinib) receives U.S. FDA approval for the treatment of patients with locally advanced or metastatic urothelial carcinoma with certain FGFR genetic alterations. https://www.jnj.com/balversa-erdafitinib-receives-u-s-fda-approval-for-the-treatment-of-patients-with-locally-advanced-or-metastatic-urothelial-carcinoma-with-certain-fgfr-genetic-alterations.
24 Kelley RK, Bridgewater J, Gores GJ, Zhu AX. Systemic therapies for intrahepatic cholangiocarcinoma. *J Hepatol*. 2020;72:353–363.
25 Kuriwaki I, Kameda M, Hisamichi H, et al. Structure-based drug design of 1,3,5-triazine and pyrimidine derivatives as novel FGFR3 inhibitors with high selectivity over VEGFR2. *Bioorg Med Chem*. 2020;28:115453.
26 Lipinski CA, Lombardo F, Dominy BW, Feeney PJ. Experimental and computational approaches to estimate solubility and permeability in drug discovery and development settings. *Adv Drug Deliv Rev*. 1997;23:3–25.
27 Doak BC, Zheng J, Dobritzsch D, Kihlberg J. How beyond rule of 5 drugs and clinical candidates bind to their targets. *J Med Chem*. 2016;59:2312–2327.
28 Mori M, Kaneko N, Ueno Y, et al. Gilteritinib, a FLT3/AXL inhibitor, shows antileukemic activity in mouse models of FLT3 mutated acute myeloid leukemia. *Invest New Drugs*. 2017;35:556–565.
29 Mori M, Ueno Y, Konagai S, et al. The selective anaplastic lymphoma receptor tyrosine kinase inhibitor ASP3026 induces tumor regression and prolongs survival in non–small cell lung cancer model mice. *Mol Cancer Ther*. 2014;13:329–340.
30 Hirano T, Yasuda H, Hamamoto J, et al. Pharmacological and structural characterizations of naquotinib, a novel third-generation EGFR tyrosine kinase inhibitor, in EGFR-mutated non–small cell lung cancer. *Mol Cancer Ther*. 2018;17:740–750.
31 Sonogashira K. Development of Pd-Cu catalyzed cross-coupling of terminal acetylenes with sp^2-carbon halides. *J Organomet Chem*. 2002;653:46–49.
32 Mitsunobu O, Yamada M, Mukaiyama T. Preparation of esters of phosphoric acid by the reaction of trivalent phosphorus compounds with diethyl azodicarboxylate in the presence of alcohols. *Bull Chem Soc Jpn*. 1967;40:935–939.
33 Tsunoda T, Yamamiya Y, Itô S. 1,1̂-(Azodicarbonyl)dipiperidine-tributylphosphine, a new reagent system for mitsunobu reaction. *Tetrahedron Lett*. 1993;34:1639–1642.
34 Ruiz-Castillo P, Buchwald SL. Applications of palladium-catalyzed C-N cross-coupling reactions. *Chem Rev*. 2016;116:12564–12649.
35 Pasto DJ, Taylor RT. Reduction of diimide. *Org React*. 1991;40:91–155.
36 Molecular Operating Environment (MOE), 2019.01; Chemical Computing Group Inc., 1010 Sherbrooke St. West, Suite #910, Montreal, QC, Canada, H3A 2R7.
37 Pronk S, Páll S, Schulz R, et al. GROMACS 4.5: a high-throughput and highly parallel open source molecular simulation toolkit. *Bioinformatics*. 2013;29:845–854.
38 Jeffrey GA. *An introduction to hydrogen bonding*. Oxford University Press; 1997.
39 Allen LC. Electronegativity is the average one-electron energy of the valence-shell electrons in ground-state free atoms. *J Am Chem Soc*. 1989;111:9003–9014.